

**UNCLASSIFIED**

**AD 406 174**

**DEFENSE DOCUMENTATION CENTER**

**FOR**

**SCIENTIFIC AND TECHNICAL INFORMATION**

**CAMERON STATION, ALEXANDRIA, VIRGINIA**



**UNCLASSIFIED**

NOTICE: When government or other drawings, specifications or other data are used for any purpose other than in connection with a definitely related government procurement operation, the U. S. Government thereby incurs no responsibility, nor any obligation whatsoever; and the fact that the Government may have formulated, furnished, or in any way supplied the said drawings, specifications, or other data is not to be regarded by implication or otherwise as in any manner licensing the holder or any other person or corporation, or conveying any rights or permission to manufacture, use or sell any patented invention that may in any way be related thereto.

63-3-6

406174

WATER AND CARBON DIOXIDE FREEZE-OUT IN  
HIGH PERFORMANCE HEAT EXCHANGERS

J. C. Burke, F. E. Ruccia, R. B. Hinckley, R. C. Reid\*

Arthur D. Little, Inc.  
Cambridge, Massachusetts

RECEIVED  
12 1963  
FEDERAL BUREAU OF INVESTIGATION  
F B I

ABSTRACT

We have conducted an analytical and experimental study to investigate the principal mechanisms of water and carbon dioxide freeze-out and to develop a method for predicting the effects of contaminant freeze-out on heat exchanger performance. This program has included an analytical study of the various mechanisms by which contaminant freeze-out may occur. A test facility was constructed having the capability of simulating a wide range of air stream pressures, temperatures, mass flow, and concentration conditions. A glass-walled test heat transfer section allowed visual and photographic observations of the frost formation as well as measurements of its effects on heat transfer and pressure drop. Based on the analytical and experimental results, the importance of the various mechanisms of contaminant freeze-out has been evaluated and a method generated for predicting the effect of contaminant freeze-out on heat exchanger performance.

The research reported herein was sponsored under a United States Air Force contract as a portion of a program to evaluate the phenomenon of heat exchanger fouling from "minor" air constituents.

---

\*Consultant and Associate Professor of Chemical Engineering at the Massachusetts Institute of Technology.

406174

## NOMENCLATURE

### SYMBOLS

A	-	flow area
$A_N$	-	area density
$A_S$	-	total heat exchanger surface area
$C_p$	-	specific heat
D	-	tube diameter
f''	-	friction factor
h	-	carrier stream film coefficient
K	-	Boltzmann's constant
k	-	thermal conductivity
L	-	heat exchanger total length
m	-	cosine of contact angle
$N_N$	-	number density
$\Delta P$	-	pressure drop
$R_c$	-	radius of critical nuclei
S	-	saturation ratio
T	-	stream temperature
$T_w$	-	wall temperature
t	-	frost thickness
$\bar{t}$	-	mean frost thickness
U	-	carrier stream overall coefficient
W	-	carrier stream flow
$W_c$	-	contaminant flow
x	-	radius ratio
X	-	heat exchanger frosted length
$\sigma$	-	surface tension
v	-	volume/molecule
$\delta$	-	tube half-clearance
$\rho$	-	density
$\theta$	-	time
$\mu$	-	viscosity

### SUBSCRIPTS

o	-	denotes zero-time condition
F	-	denotes frost property

### LIST OF FIGURES

- Fig. 1 Effect of Water Vapor Removal by Mass Transfer to Tube Wall on Saturation Ratio.
- Fig. 2 Test - Skid Viewing Side.
- Fig. 3 Test Facility Schematic.
- Fig. 4 Test Core, Wrap-Up.
- Fig. 5 Test Heat Exchanger.
- Fig. 6 Test Heat Transfer Sections
- Fig. 7 "Mass Diffusion" Deposit Formation.
- Fig. 8 Location of Freeze-out Point.
- Fig. 9 "LN<sub>2</sub> Spray" Deposit Formation.
- Fig. 10 "High  $\Delta T$ " Deposit Formation.
- Fig. 11 Typical Pressure Drop.
- Fig. 12 Pressure Drop Correlation.
- Fig. 13 Pressure Drop Correlation - LN<sub>2</sub> Spray Tests.
- Fig. 14 Heat Transfer Correlation.
- Fig. 15 Geometric Model for Single Tube Flow and Heat Transfer Analysis.
- Fig. 16 Effect of Area Blockage on Flow Capacity (Single Tube Row Analysis).
- Fig. 17 Effect of Frost Layer on Heat Transfer (Single Tube Row Analysis).
- Fig. 18 Water Frost Density.
- Fig. 19 Low-Density Water Frost Thermal Conductivity.
- Fig. 20 Thermal Conductivity of Carbon Dioxide Frost.
- Fig. 21 Overall Pressure Drop vs. Mean Area Blockage (Comparison of Simplified Hand Calculation Solution with Experimental Data).
- Fig. 22 Overall Heat Exchanger Heat Transfer Coefficient (Comparison of Simplified Analytical Solution and Experimental Data).
- Fig. 23 Comparison of Pressure Drop Test Data with Mass Diffusion Computer Program.
- Fig. 24 Comparison of Frost Thickness Profile Test Data with Mass Diffusion Computer Program.

## INTRODUCTION

Air consists of an invariable mixture of oxygen, nitrogen and other well-known constituents with variable concentrations of water vapor, carbon dioxide and other gases that may be considered contaminants. Whenever air is cooled to cryogenic temperatures, therefore, the freeze-out of water and carbon dioxide as frost will degrade heat exchanger (or other equipment) performance unless some means is provided for their removal. The overall problem of contaminant freeze-out involves both the accumulation of frost and ice within the heat exchanger and the passage of these contaminants through the heat exchanger as solid particles in the exit stream. Deposits within the heat exchanger will tend to reduce the air stream free flow area and insulate the air stream from the cold surfaces. Contaminants passing through the heat exchanger as solid particles may cause plugging in downstream components.

In many cryogenic processes, such as commercial production of oxygen, several methods to circumvent the contaminant freeze-out problem have been employed successfully. Some plants rely largely on chemical methods for removing at least the carbon dioxide while some use additional chemicals for water removal. Other processes employ metal-packed accumulators or regenerators in which both carbon dioxide and water vapor are frozen out,

subsequently to be re-evaporated by direct contact with dry exit gases. A later development to cope with the freeze-out problem employs reversing heat exchangers, in which the incoming air stream and the waste exit gases are at all times in heat exchange relation with each other. At periodic intervals, the air and waste exit gas swap channels and the waste gas removes the frost accumulation by evaporation.

Each of these systems, however, has certain inherent limitations, not the least of which is the size and weight of equipment. The reversing heat exchanger, for example, must have air and waste gas channels that are equal in heat transfer and flow areas to accommodate the low pressure waste gas during its passage through either channel.

The possible use of light weight, high performance heat exchangers for cryogenic processes involving air and its contaminants presently is under consideration. In such exchangers, tube spacing and overall size of equipment may be held to a practical minimum to achieve light weight. Degradation in performance due to flow area blockage by freeze-out, therefore, is especially severe. Further, it may be undesirable to pay the size and weight penalty necessary to equal the contaminant removal ability of commercial systems. Design of contaminant removal systems, compatible with high performance

heat exchangers, appears possible provided that the mechanism and effects of contaminant freeze-out are accurately understood.

An analytical and experimental program to investigate the principle mechanisms of water and carbon dioxide freeze-out has been undertaken. A test facility was constructed incorporating a glass-walled test heat exchanger section to permit visual and photographic observation of frost formation together with measurements of the effect of the frost on heat transfer and pressure drop. Several parameters that might affect the deposition rate of contaminants, such as air stream pressure, flow rate, water and carbon dioxide content, coolant temperature and gas to wall temperature difference, were varied during these studies to permit evaluation of their contribution to the problem. Tube diameters and tube spacings in the test section were varied to investigate the effects of heat exchanger geometry. Nucleation of the contaminants in the inlet air stream was promoted to observe the effect of impingement of particles in the heat exchanger. Based on the analytical and experimental results, the importance of the various mechanisms of freeze-out has been evaluated and a method generated to permit reasonable prediction of the effect of freeze-out on heat exchanger performance.

The research reported herein was sponsored under a United States Air Force contract as a portion of a program to evaluate the phenomenon of heat exchanger fouling from "minor" air constituents.

#### PREVIOUS STUDIES

Surprisingly few papers have been published in the area of heat transfer under frosting conditions and in all of these the only contaminant investigated was water. Kamei et al (12) froze water out in a vertical pipe cooled with brine and measured the frost properties and decrease in the rate of heat transfer. Temperatures of the air in the range of 500-510° R and, in the brine coolant, near 437° R with air velocities near 20-40 ft/sec were studied. All the water froze out on the wall by a combined eddy and diffusive mass transfer mechanism and the rates were in agreement with the usual mass transfer equations. Heat transfer rates were decreased as expected as an insulating frost layer built up. Almost dry air was used and with the small temperature differences between the air and wall, no gas phase nucleation or fogging was noted. A similar experiment was reported by Beatty et al (1) and Chen (3) although slightly higher coolant and air temperatures were employed. Prins (14) carried out some rough experiments wherein water frost was built up by blowing humid air across a bank of coolant tubes in which ammonia was vaporized. The

quantative data on rates of deposition and heat transfer reported are at best approximate but agreed with predicted estimates using mass and heat transfer equations suitable for crossflow exchangers. Three low temperature (circa 160° R) studies (10, 13, 16) were reported on liquid oxygen containers. Most of the frost formed by nucleation in the bulk vapor phase and some subsequently settled on the cold walls by a natural convection mechanism.

Probably the best work to date was reported by Chung and Algran (4). Humid air was blown over a cold tube at various angles and the rates of heat and mass transfer measured. Air temperatures near 530° R were employed and the test surface held at a near 460° R. The experiment appeared to be very well instrumented and the data again confirmed the usual mass and heat transfer rate equations. In addition to the experimental work, an analysis of the effect of frost in the rates of mass and heat transfer was presented. Finally, Hall and Tsao (9) conducted a series of heat transfer experiments in the liquid nitrogen temperature range but with water-free (and carbon dioxide free) gas. Various pressures, gas temperatures, and flow velocities were studied and the typical Nusselt-Reynolds-Prandtl number relation verified.

In all but the very low temperature studies reviewed, the experiments exercised care to minimize any gas phase nucleation, i.e., the humidities and temperature differences were maintained low enough to prevent any appreciable gas phase supersaturation. The general conclusion reached is that under these conditions, the usual mass and heat transfer rate relations are valid - if the correct surface temperatures were used in these relations.

#### ANALYTICAL SURVEY OF THE MECHANISMS OF CONTAMINANT FREEZE-OUT

The separation of a condensable component from a gas stream being cooled by contact with cold walls may occur by either of two general mechanisms. Should the cold wall be at or below the dew point of the gas, then condensation or freezing of the contaminant occurs on the walls. This local depletion of the condensable component in the gas phase causes a concentration gradient and a mass flux from the bulk gas to the wall results. Of course, simultaneously, there is a heat flux which cools the gas and if this cooling should be sufficiently rapid, the bulk gas may become saturated and lead to spontaneous nucleation of the condensable component in the bulk phase.

The driving force for mass transfer of contaminant to the walls is the concentration difference between the bulk gas and saturation concentration at the wall (or frost) - gas interface. The latter decreases exponentially with

decreasing temperature and thus reaches a value near zero for very cold walls. Thus the rate of mass transfer is a weak function of wall temperature when the latter is considerably below the dew point. However, the temperature driving force causing bulk gas cooling is almost proportional to the gas-to-wall temperature difference over a wide temperature range. This qualitative reasoning leads one to the conclusion that if the wall temperature is maintained at or slightly below the dew point temperature of the gas, most of the contaminant removal occurs by mass transfer to the walls with subsequent condensation or freezing. On the other hand, if the wall temperature is much below the dew point, then contaminant removal by mass transfer processes although increased somewhat, may be unimportant relative to the bulk phase nucleation caused by the rapid chilling of the gas.

Before discussing the various mechanisms in any detail, the forementioned ideas may be illustrated by a typical example. Suppose a water-air gas mixture at 150 psia and 620° R were cooled by flowing down a tube 0.12-inch diameter at 100 ft/sec. The coolant tube temperature varies in such a way that the difference between gas and wall is held constant over the length of the exchanger. The inlet water concentration is 4320 ppm corresponding to a dew point of 560° R under this pressure. The gas phase saturation ratio is plotted as a

function of bulk gas temperature in Figure 1. For a  $(T - T_w) = 2^\circ \text{ R}$ , the water begins to condense out at a gas stream temperature of  $562^\circ \text{ R}$  and there is sufficient mass transfer that the gas phase never reaches a saturation level greater than unity even as cooling proceeds. A similar case holds even for  $(T - T_w) = 20^\circ \text{ R}$ . When  $(T - T_w) = 60^\circ \text{ R}$ , the water removal begins at a point where the gas phase is near  $620^\circ \text{ R}$  and continues throughout the exchanger. However, for this large value of  $(T - T_w)$  there is a rapid cooling of the gas so that even though the water concentration is continually decreasing, the temperature is decreasing rapidly enough to cause a continual increase in the saturation ratio. When the gas temperature reaches about  $490^\circ \text{ R}$ , the bulk gas phase becomes saturated and bulk phase nucleation is possible. The extension of the  $60^\circ$  curve beyond  $S = 1$  has been made assuming no nucleation. In this case, over 90% of the water was removed before the bulk gas became saturated. Finally, the curve  $(T - T_w) = \infty$  indicates the limiting case of no mass transfer and, of course, the bulk gas becomes saturated at the dew point temperature of  $560^\circ \text{ R}$ .

The results shown on Figure 1 are only qualitative and based on the very simplified case where  $(T - T_w)$  is constant. Heat transfer rates were assumed proportional to this  $(T - T_w)$  and mass transfer rates to the difference between bulk gas humidity and equilibrium humidity at wall temperature. No allowance was made for any resistance to heat transfer due to the build-up of a layer of condensate or frost layer. Even with these simplifications, the trends are correct and certainly indicate that contaminant removal by a mass transfer mechanism is important for all cases except when the  $(T - T_w)$  becomes very large. This qualitative picture also leads one to predict that there would be a point of maximum contaminant removal rate corresponding to the maximum difference between gas and wall humidities. A more sophisticated model is developed in some detail later in the paper to allow for variable  $(T - T_w)$  values and the presence of frost upon the walls.

Should the bulk gas phase exceed saturation ratios of unity, there is the distinct possibility of bulk phase nucleation. If there are sufficient foreign nuclei in the gas (such as dust, salt fragments, etc.) then heterogeneous nucleation is probable and saturation ratios of only slightly greater than unity are attained. However, if the gas phase is relatively free of such foreign bodies, then nucleation will

be more homogeneous in nature and values of S greater than 5 or 10 may be attained before any appreciable nucleation is achieved.

The mechanism of homogeneous nucleation has been discussed thoroughly in the literature (2, 5, 7, 15, 19) but it is still difficult to obtain a reliable value of the rate in any given situation. Generally, the theory indicates that the rate of formation of nuclei per  $\text{cm}^3\text{-sec}$  is given as:

$$\text{rate} = K_1 \exp - \frac{16}{3} \pi \frac{\sigma^3 v^2}{(KT)^3 (\ln S)^2} \quad (1)$$

where  $K_1$  is a constant in the range of  $10^{21}$  to  $10^{25}$ ,  $\sigma$  is the surface tension of the nuclei,  $\text{ergs}/\text{cm}^2$ ,  $v$  is the volume/molecule in the nuclei,  $\text{cm}^3/\text{molecule}$ ,  $K$  is Boltzmann's constant,  $1.38 \times 10^{-16}$   $\text{ergs}/\text{molecule} \text{ } ^\circ\text{K}$ ,  $T$  the absolute temperature,  $^\circ\text{K}$ , and  $S$  the saturation ratio. The rate of formation of nuclei is very sensitive to temperature and saturation level. It is generally assumed that an "appreciable" rate of nuclei formation occurs when  $10^5$  nuclei/ $\text{cm}^3\text{-sec}$  are formed. For water air mixtures such rates occur near  $S = 5$  at  $473^\circ\text{R}$ ,  $S = 10$  at  $420^\circ\text{R}$  and  $S = 20$  at  $384^\circ\text{R}$ . Thus a cold gas with little water may be expected to sustain larger supersaturations before nucleating.

The actual nucleation process removes very little contaminant as each nuclei may contain less than 100 molecules. However, as the nuclei grow, they may rapidly deplete the gas stream and lower the saturation value to near unity. Courtney (5) has analyzed this growth process and calculated the rate of depletion for many typical cases assuming isothermal systems. The difficult problem to analyze, however, results from the competing mechanisms of growth and further nucleation for any gas stream which is being cooled. If cooling is rapid, then nucleation predominates and one finds enormous numbers of small particles. For slow cooling, the growth process limits further nucleation and large particles can be formed. At the present time, there is no adequate way to handle this general case analytically.

Heterogeneous nucleation has been analyzed by Fletcher (6) and the rate of formation of such nuclei is given by Equation (1) multiplied by the grouping:

$$A_N N_N \exp - \left[ f(m, \kappa) \right] \quad (2)$$

where  $A_N$  and  $N_N$  are the areas and number density of the foreign nuclei and  $f(m, \kappa)$  a function of  $m$ , the cos of the contact angle of contaminant deposited on the foreign nuclei, and  $\kappa$ , the ratio of the radius of the foreign particle to the radius of a critical sized homogeneously formed nuclei  $R_c$ .  $R_c$  is given

approximately as  $(2 \sigma v / kT \ln S)$  where the terms have the same meaning as in Equation (1); typical values are very small, i.e., for water-air systems at  $420^{\circ}$  R, if  $S = 10$ ,  $R_c \sim 6 \text{ \AA}$  and if  $S = 1.1$ ,  $R_c \sim 150 \text{ \AA}$ . Thus, for any reasonably sized foreign particles,  $x$  is very large and it may be shown that

$$f(r, x) = \frac{(2 + m)(1 - m^2)^2}{2} \quad (3)$$

$$x \longrightarrow \infty$$

The most effective particle is one which has a contact angle approaching unity, i.e.,  $m$  approaches unity, and  $f(m, x)$  approaches zero. This type of particle is completely wetted by the condensable component.

Although the theory of heterogeneous nucleation is well defined, it is not practicable to use the theory directly since values of  $m$  are not known. In fact, there is no general agreement as to what are "effective" nuclei to induce nucleation. Often materials which may be expected to be wettable are not effective nucleating agents (11, 15, 17, 18). About all one can conclude at the present time is that if effective nucleating particles are present, nucleation rates are rapid even for very low values of supersaturation and the resulting particles may grow to reasonable size.

### EXPERIMENTAL PROGRAM

An experimental facility was constructed to study the freeze-out of water and carbon dioxide from an air stream at temperatures down to 50° R. Freeze-out was accomplished with each of three counterflow heat exchangers consisting of both in-line and staggered tube configurations. The air stream was simulated with nitrogen gas that acted as the carrier when contaminated with known amounts of water vapor and carbon dioxide. This stream was made to flow normal to the outside of the tube elements; the refrigerant flow was inside of the tubes. The heat exchangers were mounted in a glass shell which permits the tube elements to be viewed and photographed under all test conditions.

The test facility was designed for heat exchanger carrier gas inlet pressures in the range of 30 to 300 psia, carrier mass velocities in the range 10 to 100 lbs/sec/ft. sq., and coolant inlet temperatures down to 50° R. The test facility carrier and coolant streams were supplied from high pressure cylinder manifolds. Coolant inlet temperature control was obtained in an auxiliary cryogenic heat exchanger. Provisions were included for a liquid nitrogen stream to be injected into the carrier upstream of the heat exchanger to induce nucleation of the contaminants.

### FACILITY EQUIPMENT ARRANGEMENT

All equipment required for control and instrumentation of the facility was mounted in a test skid. The skid, shown in Figure 2, is thirteen feet long, four and a half feet high, and three feet wide. The top of the skid served as a platform for the test heat exchanger and photographic equipment. Two 20-cylinder high pressure nitrogen manifolds, which served as the source of the carrier and coolant flows, and a 500-gallon liquid nitrogen tank, which supplied refrigeration for the coolant were, for reasons of size, located apart from the skid. The principal equipment is shown schematically in Figure 3.

### STREAM CONTROL

Three basic flow streams are required for the test facility. These streams are carrier, coolant, and spray streams. All three are supplied by high pressure nitrogen manifolds. The carrier and coolant systems have a rate capacity of approximately .15 pounds per second of stream flow for a thirty-minute period and the spray stream about .03 pounds per second capacity.

Flow control and measurement of each stream is accomplished by choked orifices preceded by pressure regulators, which maintained constant flow rate throughout the test. These gas stream control stations are shown in Figure 2. Secondary

flow measurement of each stream was obtained from the known volume and pressure decay of the manifolded cylinders. The temperature control of the coolant was achieved by passing this stream through coils submerged in a liquid nitrogen bath located on the test skid. The liquid nitrogen spray stream was also cooled in a separate coil of this heat exchanger, which is supplied with nitrogen from the supply tank located in the area of the high pressure manifolds. Liquid hydrogen temperatures were achieved through use of helium gas that was passed through coils immersed in liquid hydrogen.

#### CONTAMINANT ADDITION AND MEASUREMENT

Water was added to the air stream from a positive displacement metering pump. It was heated at the injection point in the air stream to improve its rate of evaporation. A 50 cc. burette was used as the reservoir at the pump inlet to allow for measurement of the water addition to the carrier during the performance of the test. Specific humidities up to 1 percent have been achieved with this system.

Carbon dioxide was added to the air stream from a high pressure cylinder filled with one atmosphere of carbon dioxide and nitrogen at 2200 psi. This "mixing bottle" is connected in parallel with the air stream manifold and both blown down together during a test giving a controlled concentration of .05 percent by weight of carbon dioxide in nitrogen.

The water and carbon dioxide content of the heat exchanger inlet and exit streams were measured on continuous reading instruments connected to multipoint recorders. A Beckman infrared analyzer was used for the carbon dioxide concentration measurements and a Consolidated Electrodynamics Corporation humidity meter was used for measurement of the water concentration.

The gas sample streams were heated to about 910° R at the sampling points to vaporize the solid and liquid phases of the contaminants to eliminate erroneous readings resulting from contaminant accumulation in the sample lines. The sample probes at the heat exchanger inlet and exit could be rotated to face upstream or downstream in order to differentiate between vapor and solid contaminants.

#### TEST HEAT EXCHANGERS

The test heat exchanger assembly consists of an inner glass tube (either 1 inch or 2 inch) which contains the heat transfer section, surrounded by a 6-inch I.D. glass tube which insulates and prevents frosting of the inner glass. The annular space between the glass tubes is purged with dry nitrogen or helium gas. The general arrangement of these glass sections is shown in Figures 4 and 5A. In the event of failure of the outer glass and to protect operating personnel, the 6-inch glass section was surrounded with a metal hood that is vented at the

top through a screen and has a see-through section in the vicinity of test heat exchanger formed by a pane of bullet-proof glass 1-inch thick and 9-feet wide. This viewing section can be seen in Figure 2.

In the heat transfer section, the air stream flows within the annulus formed by the inner glass tube and an instrumented core. The coolant flows within tubes located in this annular space. The general direction of the air and coolant are opposite resulting in a counterflow-type heat exchanger. Three heat exchangers covering two general types of heat transfer configurations have been used in our studies. Their principal characteristics are given in Table 1.

#### SPIRAL WOUND TUBES

In this type, the coolant flows in copper tubes that are wound in a spiral that is fitted in the annular carrier gas space. The carrier flows nearly perpendicular to these tubes. Two such heat exchangers were fabricated. One of these consisted of three 3/16-inch O.D. tubes parallel wound with an outside diameter of approximately 1 inch. This configuration has been used at air stream pressures of 300 psia and coolant pressures of 1000 psi and is shown in Figures 4 and 5B.

The second heat exchanger consisted of a single 3/8-inch O.D. spiral wound tube with an outside diameter of approximately 2 inches. This unit was operated at air stream pressures of

90 psia (maximum pressure limited by 2-inch glass tube pressure rating) and 1000 psi coolant pressures. This heat exchanger is shown in Figure 6B.

#### AXIAL TUBES

In this type, the 3/16-inch O.D. coolant tubes are parallel with the center line of the inner glass tube. The air flow is baffled so as to flow perpendicular to the tubes. Air stream pressures up to 90 psia and coolant streams of 1000 psi have been used with this unit. The passages and baffle arrangement are shown in Figure 6A.

#### HEAT EXCHANGER INSTRUMENTATION

Each heat exchanger was instrumented so that the pressure and temperature of the air stream was measured at five axial locations. The coolant pressures and temperatures were measured at the inlet and outlet of the heat exchanger. Thermocouples connected to multipoint recorders were used for all temperature measurements. Coolant pressures were measured on Borden tube gauges as were the carrier stream pressures in the test heat exchanger. Three of the carrier stream pressures were also measured with transducers that were read out on multipoint recorders.

#### TEST PROGRAM

The test program was conducted to determine the effects of nine principal variables. These are listed in Table 2 with

the range over which each was investigated. Our test program was divided into four test series.

The group of tests designated as the flow series was performed with the 1-inch spiral tube heat exchanger to investigate the effect of the first six of these variables on carrier pressure, flow velocity, water and carbon dioxide content, gas to wall differential temperature, and spray to carrier ratio. In the hydrogen series, tests were performed to extend the range of inlet temperature from 140° R to 50° R. The effect of tube size and configuration was investigated in the group of tests designated as the configuration series through use of the 2-inch spiral and 2-inch staggered tube heat exchangers. The last group of tests designated as the verification test series was performed to extend the range of water concentration investigated to 1.0 percent. Further in this series, information was obtained on water and carbon dioxide frost density and stream nucleation effects that result when liquid nitrogen is sprayed into the carrier gas stream. The important parameters for each test are summarized in Table 3.

#### ANALYSIS OF TEST DATA

The primary test data consisted of photographs of the deposition in the test heat exchanger, contaminant concentration readings at the inlet and exit of the test heat exchanger, and

measurements of pressures and temperatures along the heat exchanger. From the photographs we were able to study the distribution and physical characteristics of the deposit formation. The contaminant concentration readings defined the quantity of water and carbon dioxide entering and leaving the test heat exchanger. The measurements of pressure and temperature indicated the effects of contaminant deposition on heat transfer and pressure drop.

#### PHYSICAL CHARACTERISTICS OF DEPOSIT FORMATION

For low gas-wall temperature difference ( $100^{\circ}$  R or less) the water and carbon dioxide frost accumulated as a relatively dense coating, fairly uniformly distributed around the heat exchanger tubes. The frost seemed to adhere quite securely to the tubes and no deposit migration due to shear was evident. A close-up photograph of this type of deposit formation is shown in Figure 7. The water and carbon dioxide frosts generally deposited in two distinct locations dependent on their respective saturation temperatures. As shown in Figure 8, the start of frosting correlated quite well with the points at which the tube wall temperature reached the saturation temperature corresponding to the inlet contaminant concentration. It was found that, in general, the bulk of the deposition was complete by the location at which the carrier stream temperature had dropped to saturation at 10% of the inlet contaminant

concentration. Measurements of frost thickness, obtained from close-up photographs indicated that the frost thickness increased to a maximum after the start of frosting and then decreased again. As will be shown later, this distribution is in accordance with the thickness distribution indicated by mass transfer theory. From the measurements of frost thickness and the known quantity of inlet contaminant it was possible to estimate the frost density. The density of water frost was found to be approximately .25 gm/cc; the carbon dioxide density, approximately 1 gm/cc.

In tests in which liquid nitrogen was injected into the inlet carrier stream, nucleation was induced in the bulk gas stream. In this situation, the frost formed as particles in the bulk stream was subsequently entrapped in the heat exchanger by impingement. This deposit formation appeared to be less dense and less adherent than that resulting from mass transfer. Migration of the frost due to gas shear was evident. A close-up photograph of this type of deposit formation is shown in Figure 9. It appeared that particle size, as controlled by liquid nitrogen spray rate, was the predominant factor influencing frost distribution. Low liquid nitrogen spray rates induced low saturation ratios favoring the formation of a small number of relatively large particles. These large particles

were readily separated by impingement causing the frost to be concentrated near the inlet of the heat exchanger. High liquid nitrogen spray rates induced high saturation ratios favoring the formation of a large number of extremely small particles. These small particles were less susceptible to impingement separation and as a consequence the frost was distributed over a large percentage of the heat exchanger area.

In tests at high gas-wall temperature differences (approximately 200° R) the mechanisms of both mass transfer and nucleation were important. The resulting deposit formation was a combination of the effects of mass transfer to the wall and nucleation in the bulk stream with subsequent attachment by impingement. A close-up photograph of this type of deposit formation is shown in Figure 10.

#### CONTAMINANT CONCENTRATION IN HEAT EXCHANGER EXIT GAS

Measurements of the contaminant composition in the exit gas have indicated that the major portion of the inlet contaminant accumulates as frost in the test heat exchanger. Generally, the exit contaminant composition was found to be near saturation at the exit temperature, for carbon dioxide and also for water at relatively high exit temperatures. However, for water at low exit temperatures, it was usually impossible to measure the actual exit concentration since the test instrumentation could not go below about 10 ppm.

From mass transfer theory, it would be expected that at low gas-wall temperature differences, the exit gas would contain only contaminant in the vapor phase at a concentration equal to or less than saturation. In the presence of bulk stream nucleation, caused either by a high gas-wall temperature difference or by liquid nitrogen spray, some particle carry through might be anticipated. However, test results have indicated that even when such nucleation was induced very little contaminant was present in the exit gas. Evidently, under our test conditions, the heat exchanger core is quite efficient as an impingement separator for removing solid particles. This result has been demonstrated for both in-line and staggered tube heat exchanger configurations.

#### PRESSURE DROP

All the tests described in this paper were conducted at constant air flow. Therefore, the increase in pressure drop across the test heat exchanger was a measure of the degradation of heat exchanger flow area due to deposit formation.

Pressure taps spaced at intervals along the test heat exchanger indicated the distribution of pressure drop as well as the overall heat exchanger pressure drop. In all cases, the regions of high pressure drop coincided with the regions in which the frost thickness was a maximum. It was also found that in most tests the pressure drop due to water frost was much

greater than the pressure drop due to carbon dioxide frost - even when the mass addition of carbon dioxide was equal to or somewhat greater than the mass addition of water. This seeming inconsistency is due to the lower density (or greater specific volume) of the water frost compared to the carbon dioxide frost. In a limited number of tests in which the water content was reduced to a minimum, it was possible, however, to develop high pressure drops due to carbon dioxide frost.

Typical plots of heat exchanger pressure drop as a function of the contaminant deposition time are shown in Figure 11. The tests represented on this plot were similar in all respects except for the concentration of water. In this particular group of tests, no carbon dioxide was present; therefore, the pressure drop increase was solely due to accumulation of water frost. The result shows that the rate of pressure drop increase is strongly dependent on inlet air water content. Inspection of Figure 11 indicates that, at any level of pressure drop appreciably above the clean heat exchanger pressure drop, the product of the percent water and water addition time for the various tests is approximately equal. Therefore, the data might be expected to fall into a single curve if plotted against water addition mass. The water addition mass has, in fact, been

found to be a good correlating parameter for a large portion of the test data. However, as discussed below, it is advantageous to utilize a somewhat more general correlation scheme which also accounts for variations in heat exchanger area and frost density.

In correlating the pressure drop data, it was found convenient to plot the ratio of frosted heat exchanger pressure drop to clean heat exchanger pressure drop as a function of the mean area blockage. The mean area blockage parameter serves to generalize the effects of deposition time, contaminant flow rate, heat exchanger surface area, tube clearance, and frost density. This parameter is calculated by the equation.

$$\bar{t}/\delta_o = \frac{\int_0^{\theta} wcd\theta}{\rho_F A_s} \quad (4)$$

where:

- $\bar{t}$  = mean frost thickness
- $\delta_o$  = tube half clearance
- $\int_0^{\theta} wcd\theta$  = total contaminant mass addition
- $\theta$  = contaminant addition time
- $\rho_F$  = frost density
- $A_s$  = total heat exchanger surface area

A plot of pressure drop ratio vs. mean area blockage is presented in Figure 12. This plot includes data for a wide range of operating conditions including variations in pressure, flow velocity, coolant inlet temperature and contaminant concentration. These tests do not include liquid nitrogen spray or low enough concentrations of water to allow the carbon dioxide pressure drop increase to be significant. It was found from this plot that tests having approximately equal "frosted lengths" fell along a single plot. For instance, all the data of Figure 11 fell close to a single curve. Reducing "frosted length" served to increase pressure drop at a constant value of area blockage.

In computing the frosted length fraction ( $X/L$ ), it was assumed that the start of frosting corresponded to the point at which the wall temperature reached the inlet contaminant saturation temperature. The end of the frosted length was defined as the location at which the carrier gas temperature had dropped to saturation at 10% of the inlet contaminant concentration.

A similar correlation plot is presented for liquid nitrogen spray tests in Figure 13. In this case, a frosted length computed from temperature profiles has little significance since the contaminant deposition involves nucleation rather than mass transfer. This plot indicates that the pressure drop ratio is

reduced by increasing liquid nitrogen spray rate. This result is in accordance with the photographic and visual evidence indicating that higher spray rates resulted in more uniform frost distribution throughout the heat exchanger and consequently greater frosted lengths.

#### HEAT TRANSFER

Our test results have indicated very little change in overall heat flow due to deposit formation. In a large measure, this is due to the fact that in an efficient (i.e., low heat transfer  $\Delta T$ ) heat exchanger, an appreciable reduction in heat transfer coefficient will result in a small change in overall heat flow. By way of further explanation, it may be noted that in a counterflow heat exchanger, the maximum heat flow, corresponding to infinite heat transfer coefficients, is a function of the inlet temperatures and flow rates of the hot and cold fluids. The actual heat flow increases with increasing heat transfer coefficient and approaches this maximum as an asymptote. However, in the asymptotic region of a plot of heat flow versus heat transfer coefficient, the heat flow is a relatively weak function of heat transfer coefficient.

Calculation of heat transfer coefficients from the test data were inherently rather inaccurate, since the error in the fluid temperature measurements was an appreciable portion of the

heat transfer  $\Delta T$ . A typical plot of heat transfer coefficient ratio (frosted over clean) vs. mean area blockage is presented in Figure 14. Although the data has appreciable scatter, this plot indicates that the changes in overall heat exchanger heat transfer coefficient are much less, for comparable area blockage, than the changes in pressure drop.

ANALYTICAL METHODS FOR PREDICTING THE EFFECTS OF CONTAMINANT DEPOSITS ON HEAT EXCHANGER PERFORMANCE

As a first step in considering the effects of contaminant deposition on heat exchanger performance, it is useful to investigate the effect of a frost layer of given thickness and thermal conductivity on the flow and heat transfer capacity of a single tube row. The geometric model for this analysis, consisting of adjacent tubes separated by clearance  $2\delta_0$  and coated with a frost thickness  $t$  is shown in Figure 15.

The pressure drop across the tube row is directly proportional to flow per unit area and inversely proportional to fluid density. Therefore, making use of the geometric relationships of Figure 15, the pressure drop ratio may be written as:

$$\frac{\Delta P / \Delta P_0}{(w/w_0)^2} = \left[ \frac{1}{1 - t/\delta_0} \right]^2 \rho_0/\rho \quad (5)$$

where:

$\Delta P$      $\curvearrowright$  pressure drop  
w         $\curvearrowright$  flow rate  
t         $\curvearrowright$  frost thickness  
 $\delta$         $\curvearrowright$  tube half clearance  
 $\rho$         $\curvearrowright$  fluid density

subscript<sub>o</sub> represents clean conditions.

Similar, although slightly more complex, relationships can be developed to relate variations in the carrier stream over-all heat transfer coefficient, ( $u$ ), which includes both gas film resistance and frost resistance, to area blockage ( $t/\delta_o$ ) and a "frost Nusselt number" ( $h_o \delta_o/kF$ ) based on the initial carrier side film coefficient,  $h_o$ , the tube half clearance,  $\delta_o$ , and the frost thermal conductivity  $kF$ .

For close packed tubes (pitch/diameter  $\leq 1.4$ ) the ratio of over-all carrier stream heat transfer coefficients may be written as:

$$\frac{u_o}{u} = (1 - t/\delta_o)^6 (w_o/w)^6 + (h_o \delta_o/kF) (t/\delta_o) \quad (6)$$

The derivation of these equations is presented in Appendix I. The results are plotted in Figures 16 and 17. These plots show that, for constant flow density, the pressure drop parameter is a single valued function of area blockage, increasing as area blockage increases. This relationship is independent of whether

the system is constant flow or constant pressure drop. The heat transfer parameter is dependent on the "frost Nusselt number", area blockage and the system operating line. For constant pressure drop the heat transfer coefficient must always decrease - the rate of decrease being dependent on the frost Nusselt number. High values of frost Nusselt number (i.e., low frost thermal conductivity) result in a rapid decrease in heat transfer. For constant flow, the over-all heat transfer coefficient may actually increase if the frost thermal conductivity is high, since the increased film coefficient associated with reduced flow area outweighs the insulating effect of the frost. For the tests conducted in this program the frost Nusselt number was of the order of 5.0. Therefore, frost formation would be expected to reduce the over-all carrier gas coefficient.

The single tube analysis has illustrated, in a qualitative manner, the effects of frost thickness and thermal conductivity on heat exchanger performance. In considering an actual heat exchanger in which frost thickness varies along the heat exchanger, it is necessary to know the distribution of frost thickness so that the flow and heat transfer effects can be integrated along the length of the heat exchanger. Therefore, an analytical approach requires methods of determining both frost distribution and frost properties.

Analytical and experimental results indicate that mass transfer is the most important mechanism governing the distribution of contaminants in heat exchangers. This admitted generalization is most valid when the heat exchanger  $\Delta T$  between air and coolant is small. However, test results have indicated that even with quite large  $\Delta T$ 's in the order of 200° R the deposition of contaminants in the heat exchanger is not greatly different and the pressure drop not substantially different than would result from mass diffusion. Surprisingly enough, even in the presence of nucleation due to liquid nitrogen spray, which does make a substantial difference in the texture and distribution of deposits, the pressure drop effect does not appear to be grossly different than that which would exist in the presence of a mass transfer type of deposit. Therefore, we have concluded that the mass transfer mechanism is the most practical mechanism to serve as a basis for an analytical model of frost distribution.

From a literature search and results of the present program, a correlation plot of water frost density vs. velocity has been prepared. This correlation, shown in Figure 18, indicates a water frost density of about .25 gm/cc at a nominal air side velocity of 60 ft/sec. No data is available in the literature on carbon dioxide frost density. Experimental results have indicated a density of about 1 gm/cc at a nominal air velocity of

60 ft/sec. For lack of further information, we will assume this density value is typical for high performance heat exchangers.

A study has been conducted to determine the most appropriate methods to relate frost thermal conductivity to the frost density, structure and properties of the constituents making up the frost. It was concluded that for reasonably low density frosts (i.e.,  $\rho_F < 0.5 \rho_{\text{solid}}$ ) Woodside's model (20) yields the best agreement with experimental data. For high density frosts, Riemann's (8) truncated sphere model seems appropriate. Using these models, generalized plots have been prepared for determining water and carbon dioxide frost thermal conductivities from given frost density values. These plots are presented in Figures 19 and 20.

Both computer solutions and hand calculation methods have been considered for predicting deposit accumulation and the resultant effects on heat exchanger performance. Both approaches require prior knowledge of water and carbon dioxide density and thermal conductivity. The computer solution is potentially capable of developing accurate frost profiles from mass transfer theory and integrating the pressure drop and heat transfer effects along the heat exchanger as part of a unified calculation procedure with a minimum of simplifying assumptions.

In order to avoid extended tedious calculations, it is generally necessary to employ some rather arbitrary assumptions regarding frost distribution in the hand calculations techniques. It has been concluded that both methods have value. Hand calculation techniques are useful as a simple, flexible, means of approximating the effects of contaminant deposition on heat exchanger performance and as a basis for data correlation techniques. On the other hand, computer solutions are generally required for maximum calculation accuracy, especially in those cases in which heat exchanger inlet conditions are varying.

A simplified hand calculation analysis based on the assumption of uniform frost thickness within an effective frosted zone has been valuable in analyzing and correlating test data. The assumption of uniform frost thickness in a frosted zone allows the area blockage in that zone to be calculated readily. Knowing the area blockage, the degradation in flow capacity and heat transfer in the frosted zone can be determined from Figures 16 and 17. The overall changes in flow capacity and heat transfer for the heat exchanger can in turn be obtained by combining the performance of the clean and frosted sections. Following this basic approach, Figure 21 presents overall heat exchanger pressure drop as a function of mean area blockage and frosted length fraction. This parametric presentation is similar to that used for correlating the pressure

drop data. As previously pointed out, the frosted length fraction can be computed from the heat exchanger temperature profiles. Also plotted on Figure 21 are the test data originally presented in Figure 11. The experimental data is in at least qualitative agreement with the analytical curve for a comparable frosted length fraction ( $.33 < X/L < .37$ ). It may also be noted that the analysis shows the effect of  $X/L$  on pressure drop ratio to be similar to that shown in the pressure drop data correlation of Figure 12. Figure 22 presents a comparison of experimental and analytical heat transfer results for the test data originally presented in Figure 14. The analytical and experimental data indicate about the same rate of heat transfer decay.

#### COMPUTER SOLUTION

Temperatures and pressures vary both with time and position in the heat exchanger. To allow for such variations, material, momentum, and energy balances are written in differential form along with the appropriate heat transfer rate expressions and solved as a function of length for the clean exchanger. This zero-time solution established temperature and pressure profiles for the carrier gas, and the temperature profile for the coolant. The wall temperature gradient and heat flux were then calculated. With these values established,

one then assumes that the entering carrier gas is instantaneously contaminated with some pre-set water and carbon dioxide concentration. By following a control volume of this gas down the heat exchanger, the rates of mass transfer to the wall were estimated and the humidity profiles determined.

With these data, one chooses an appropriately small time increment and determines frost depositions along the heat exchanger. At the end of this time increment, the frost mass deposited in any differential length was converted to a thickness using the frost density-velocity correlation described earlier. The differential momentum balance equations were then solved to yield a new pressure profile and the energy balance and heat transfer equations solved to yield new temperatures; in the latter, account must now be taken of the thermal resistance of the frost layer employing the calculated thickness and estimated frost conductivity. As before, then, new mass transfer fluxes were estimated, and the next time step chosen.

This step-wise iteration technique is continued until the end of the test or until some predetermined pressure drop is attained. The tediousness of the calculations necessitated the use of a high-speed IBM 7090 computer.

From such a method, it is possible to print-out at any time the pressure and temperature gradients in the coolant and carrier stream, the wall and frost carrier gas interface temperature gradients, the humidity gradients, and the frost distribution profile. Variable inlet conditions may be handled by this technique.

Preliminary results on a simplified version of this computer program, which neglects heat transfer variations and is adaptable only to constant flow operation are shown in Figure 23 and Figure 24. Figure 24 indicates that the computer program, based on mass diffusion theory, is quite successful in predicting frost thickness distribution. The pressure drop comparison of Figure 23 also indicates general agreement between analysis and experiment, although the analytical pressure drop appears to increase more slowly near the start and more rapidly later in the test than does the experimental result.

#### CONCLUSIONS

1. For  $\Delta T$  of  $100^{\circ}$  R or less, the deposit formation is relatively a dense adherent material - more or less uniformly distributed around tubes. Axial frost distribution appears to be in accordance with mass transfer theory.

2. In the presence of liquid nitrogen spray or a high gas-wall  $\Delta T$  ( $\Delta T \geq 200^\circ \text{R}$ ) freeze-out may occur in the bulk gas stream due to nucleation. The resulting deposit, which forms on heat exchanger tubes by impingement, appears lighter in density and tends to migrate. When the saturation ratio is of the order of 5, large particles are formed which plug the front end of the heat exchanger. At saturation ratios greater than 10, the nucleated particles appear to distribute over a significant length of heat exchanger.

3. In all tests, a major portion of deposit accumulated in heat exchanger. Exit contaminant concentrations were generally near saturation.

4. The measured frost density is of the order of .25 gm/cc for water frost; 1 gm/cc for carbon dioxide frost. Methods have been developed for estimating frost thermal conductivity from known density values.

5. Pressure drop and heat transfer results appear to be in general accordance with the computed area blockage and frost insulation.

6. A digital computer solution based on mass transfer theory appears to be well suited to predicting the effects of contaminant deposition on heat exchanger performance. A preliminary version has been successful in predicting the frost distributions and heat exchanger pressure drop.

### ACKNOWLEDGEMENT

The authors wish to acknowledge the many and significant contributions made by the other members of the program task force. Particularly to E. M. Drake, who developed the mass diffusion model for freeze-out of water vapor; to R. P. Berthiaume for the design and development of heat exchanger glass housings and support system; to M. Weber for setting up the mass and heat transfer and pressure drop equations for computer application; to I. W. Dingwell for carrying out the computer program; and to J. Franklin for assistance in setting up and operating the experimental equipment.

### BIBLIOGRAPHY

1. Beatty, K. O., E. B. Finch, and E. H. Schoneborn, Sept. 11-13, General Discussion on Heat Transfer, ASME-IRE, London, 1951.
2. Becker, R., and Doring, W., Ann. Physik 24, 719 (1935).
3. Chen, M. M., Ph.D. Thesis, Mech. Eng., M.I.T., Cambridge, Mass., 1960.
4. Chung, P. M., and A. B. Algren, Heating, Piping and Air Conditioning 30, No. 9, 171; No. 10, 115 (1958).
5. Courtney, W. G., and Clark, W. J., "Kinetics of Condensation from the Vapor Phase", Texaco Exp., Inc. TM-1250.
6. Fletcher, N. H., J. Chem. Phys. 29, 572 (1958).

7. Frenkel, J., "Kinetic Theory of Liquids", Dover Pub., Inc., New York, 1955.
8. Gorring R. L., and Churchill, S. W., Chem. Eng. Prog. 57, 53 (1951).
9. Hall, T. A., and Tsao, P. H., Proc. Roy. Soc. (London) A191, 6, (1947).
10. Holten, D. C., B.S. Thesis, Univ. of Colorado, 1957.
11. Izmailova, G. I., P. S. Prokhorov, and B. V. Peruagin, Coll. J. (USSR) 19, 557 (1957).
12. Kamei, S., T. Mizushina, S. Kifune, and T. Koto, Chem. Eng. (Japan) 14, No. 1, 53 (1950).
13. Loper, J. L., Trans. ASHRAE 66, 104 (1960).
14. Prins, L., Kaltetechnik 8, 160, 182 (1956).
15. "The Physical Chemistry of Aerosols", Disc. Faraday Soc. No. 30, (1960), p. 20, 39, 145, 376.
16. Ruccia, F. E., and C. M. Mohr, "Atmospheric Heat Transfer to Vertical Tanks Filled with Liquid Oxygen", Proc. of the 1958 Cryogenic Eng. Conf., Cambridge, Mass., Sept. 3-5, 1958.
17. Schaefer, V. J., Ind. Eng. Chem 44, 1300 (1952).
18. Turnbull, D., and B. Vonnegut, Ind. Eng. Chem. 44, 1292 (1952).
19. Volmer, M., "Kinetik der Phasenbildung", Edwards Bros. Ann Arbor, 1945.
20. Woodside, W., Can. J. Physics 36, 815 (1958).

TABLE I

HEAT EXCHANGER DATA

Heat exchange. configuration	1" spiral tube	2" spiral tube	2" staggered tube
Heat exchanger length (in)	49	48	37
No. of parallel coolant tubes	3	1	20
Coolant tube O.D. (in)	3/16	3/8	3/16
Coolant tube wall thickness (in)	.030	.032	.032
Total air side surface area (ft <sup>2</sup> )	1.76	4.4	3.0
Air to coolant surface area ratio	1.472	1.205	1.535
Air side flow area (in <sup>2</sup> )	.150	.310	.278
Coolant side flow area (in <sup>2</sup> )	.0379	.0762	.234
Air to coolant flow area ratio	3.96	4.08	1.19
Average distance of the tubes from the glass wall and instrument core (in)	.031	.031	.035

TABLE 2  
VARIABLES INVESTIGATED

	<u>Range</u>
1. Pressure (psia)	15 to 300
2. Flow velocity (ft/sec)	25 to 80
3. Water content (wt. percent)	.001 to 1.0
4. Carbon dioxide content (wt. percent)	0 and .05
5. Gas to wall differential temperature ( $^{\circ}$ R)	5-200
6. Ratio liquid nitrogen spray flow/carrier flow	.2 to .46
7. Coolant tube O.D. (in)	3/16 and 3/8
8. Tube configuration	In-line and staggered
9. Coolant inlet temperature ( $^{\circ}$ R)	410 to 50
10. Air inlet temperature ( $^{\circ}$ R)	520 to 560

TABLE 3

## TEST PARAMETER SUMMARY

Test No.	Carrier				Coolant		Spray	Variables (1) Investigated
	Mass Flow ( $\frac{\text{lbs}}{\text{sec-ft}^2}$ )	Inlet Pressure ( $\frac{\text{lbs}}{\text{in}^2}$ )	H <sub>2</sub> O conc. (%)	CO <sub>2</sub> conc. (%)	Inlet Temp. (°R)	Heat Ratio ( $\frac{\text{WC}_p}{\text{WC}_p}$ )	Mass Ratio $\frac{W_s}{W_a}$	
F-1	10	30	.005	0	260	1.0	-	1
F-2	30	90	.006	0	304	1.0	-	3
F-3	30	90	.026	0	304	1.0	-	3
F-4	30	90	.045	0	304	1.0	-	3
F-5	30	90	.052	0	304	1.0	-	3
F-7	30	90	.001	.05	170	1.0	-	5
F-8	30	90	.016	.05	170	1.0	-	5
F-9	30	90	.020	.05	170	.5	-	5
F-12	30	90	.018	.05	150	2.0	-	5
F-10	50	90	.018	.05	170	1.0	-	2
F-11	15	90	.030	.05	180	1.0	-	2
F-13	39(2)	90	.012	.05	170	1.0	.33	6
F-14	37(2)	90	.012	.05	170	1.0	.25	6
F-17	100	300	.017	.05	150	1.0	-	1
H-1	30(4)	90	min	.05	160	1.0	-	system check run
H-2	30(4)	90	min	.05	50	1.0	-	1, 4
H-3A	30	90	min	.05	50	1.0	-	1, 4
H-4	13	90	min	.05	50	2.3	-	1, 4
H-5	30	90	min	.05	50	1.75	-	1, 4
H-6	30	90	.025	.05	50	1.75	-	1, 4, 5
C-1	30	90	.025	.05	160	1.0	-	5, 8
C-2	39(2)	90	.025	.05	160	1.0	.2	6, 8
C-3	30	90	.025	.05	150	2.0	-	5, 8
C-4	37(2)	90	.025	.05	150	1.0	.35	6, 8
C-5	30	90	.025	.05	160	1.0	-	7, 8
C-6	30	90	.025	.05	160	2.0	-	7, 8
V-1	10	30	.025	.05	190	1.0	-	1, 3, 4
V-2	30	90	.1	-	300	1.0	-	3
V-3	30	90	.32	.05	305	1.0	-	3
V-4	10	30	1.0	.05	180	1.0	-	3
V-5	30	90	.027	-	410	1.0	-	3
V-6	30	90	neg	.05	160	1.0	-	4
V-7	30	90	neg	.044	165	1.0	-	4
V-8	15	90	.025	.047	170	1.0	-	2
V-9	35(2)	90	.029	.046	175	1.0	.46	6

## NOTES:

- Numbers refer to variable designations given in Table 2.
- Mass flow is based on the sum of the carrier and spray streams.
- Tests C-1 through C-4 were performed with 2-inch staggered tube heat exchanger and test C-5 and C-6 were performed with 2-inch spiral tube heat exchanger.
- Equivalent volumetric helium flow.

## APPENDIX I - SINGLE TUBE ROW ANALYSIS

The presence of a frost layer degrades heat exchanger flow capacity by reducing the free flow area. The effect of the frost layer on heat transfer depends on both the area blockage and thermal insulation of the deposits. The thermal insulation of the frost tends to reduce heat transfer. The area blockage effect, however, tends to increase the air-side film heat transfer coefficients by increasing flow velocities.

Consideration of the effects of a given thickness and thermal conductivity of a frost layer on a single tube row illustrates the effects of frost on heat exchanger performance. For this analysis, the heat transfer and flow geometry are defined in Figure 15.

### A. Flow and Pressure Drop

For a single tube row, the flow-pressure drop relationship, per reference 1, may be expressed as:

$$\Delta P = 4f'' \frac{(W/A)^2}{\rho} \quad (A-1)$$

Neglecting variations in friction factors, the ratio between frosted pressure drop and clean pressure drop may be written as:

$$\Delta P / \Delta P_0 = (W/W_0)^2 (A_0/A)^2 \rho_0 / \rho \quad (A-2)$$

The above equation shows that the air pressure drop is directly proportional to the square of the flow rate, inversely proportional to the square of the free area, and inversely proportional to the fluid density. Since, referring to Figure 15, it is seen that free area is portional to the available "half clearance" between tubes ( $\delta = \delta_0 - t$ ), the flow-pressure drop relationship also may be expressed as:

$$\frac{\Delta P / \Delta P_0}{(W/W_0)^2} = \left[ \frac{1}{1 - t/\delta_0} \right]^2 \frac{\rho_0}{\rho} \quad (A-3)$$

where:

- $\Delta P$      $\curvearrowright$     pressure drop
- $W$          $\curvearrowright$         flow rate
- $t$           $\curvearrowright$         frost thickness
- $\delta$           $\curvearrowright$         tube half clearance
- $\rho$           $\curvearrowright$         fluid density

subscript<sub>0</sub> represents clean conditions

A plot of the above relationship, for constant flow density, is presented in Figure 16. This plot indicates that an area blockage of 10% at a tube row would either increase the pressure drop across the tube row by 25%, for a constant flow system, or reduce the flow by 10%, for constant pressure drop across the tube row. The stipulation of constant flow density

is probably valid for most practical applications in which substantial pressure or density variations due to deposit formation could not be tolerated.

B. Heat Transfer

The overall air-side heat transfer coefficient  $u$ , is including air side film resistance and the deposit insulation, for the single tube row of Figure 15, may be written as:

$$1/u = 1/h + t/k_f \quad (A-4)$$

where:

- $u$  ~ overall air side heat transfer coefficient
- $h$  ~ air-side film heat transfer coefficient
- $t$  ~ frost thickness
- $k_f$  ~ frost thermal conductivity

For the "clean" tube row ( $t = 0$ ) this equation reduces to  $u_o = h_o$ . Therefore, the ratio of clean to frosted overall heat transfer coefficient may be written as:

$$u_o/u = h_o/h + h_o t/k_f \quad (A-5)$$

The air side film heat transfer coefficient ( $h$ ) may be related to flow, tube diameter, and fluid properties by the following equation valid for flow normal to tubes.

$$\frac{hD}{k} = .33 \left( \frac{D W/A}{\mu} \right)^{.6} \left( \frac{c_p \mu}{k} \right)^{1/3} \quad (A-6)$$

Neglecting variations in air stream thermal conductivity, viscosity, or Prandtl number during the frosting process, we may express the ratio of clean to frosted air side film coefficients as:

$$h_o/h = (D/D_o)^{.4} (W_o/W)^{.6} (A/A_o)^{.6} \quad (A-7)$$

The tube diameter ratio  $(D/D_o)$ , and free flow area ratio  $(A/A_o)$  may be written as:

$$\frac{D}{D_o} = \frac{D_o + 2t}{D_o} = 1 + 2t/D_o = 1 + 2(t/\delta_o) (\delta_o/D_o) \quad (A-8)$$

$$\frac{A}{A_o} = \frac{\delta}{\delta_o} = \frac{\delta_o - t}{\delta_o} = 1 - t/\delta_o \quad (A-9)$$

It is also convenient to rewrite the parameter  $h_o t/k_f$  as  $(h_o \delta_o/k_f) (t/\delta_o)$ . Therefore, the ratio of clean to frosted overall air-side heat transfer coefficient may now be written as:

$$u_o/u = \left[ 1 + 2(t/\delta_o) (\delta_o/D_o) \right]^{.4} 1 - t/\delta_o^{.6} (W/W_o)^{.6} + (h_o \delta_o/k_f) (t/\delta_o) \quad (A-10)$$

This equation shows the variation in overall air side heat transfer coefficient is a function of  $\delta_o/D_o$ ,  $t/\delta_o$ ,  $W/W_o$  and  $h_o \delta_o/k_F$ . For close packed tubes, little error results if we assume that  $\delta_o/D_o = 0$  or more specifically that  $\left[1 + (t/\delta_o) (\delta_o/D_o)\right]^{.4} \approx 1.0$ . As a test of this assumption, assume a pitch to diameter ratio of 1.4 (or  $\delta_o/D_o \approx .2$ ) and compare the term  $\left[1 + 2(t/\delta_o) (\delta_o/D_o)\right]^{.4}$  with the term  $\left[1 - t/\delta_o\right]^{.6}$  as a function of  $t/\delta_o$ .

$t/\delta_o$	$\frac{1 + 2(t/\delta_o) (\delta_o/D_o)^{.4}}{}$	$\frac{1 - t/\delta_o}{.6}$
.1	1.016	.9385
.2	1.031	.875
.5	1.076	.66

This comparison shows that for close packed tubes, the term  $\left[1 + 2(t/\delta_o) (\delta_o/D_o)\right]^{.4}$  is very nearly equal to unity. Therefore, the ratio of clean to frosted air side overall heat transfer coefficients may be approximated with relatively little error as:

$$u_o/u = (1 - t/\delta_o)^{.6} (W_o/W)^{.6} + (h_o \delta_o/k_F) (t/\delta_o) \quad (A-11)$$

The above relationship is valid for constant pressure drop, constant flow, or any immediate operating lines. Certain simplifications can be made, however, for the specific cases of constant flow or constant pressure drop across a single tube row. For constant flow ( $W/W_o = 1.0$ ):

$$u_o/u = (1 - t/\delta_o)^{.6} + (h_o \delta_o/k_p) (t/\delta_o) \quad (A-12)$$

For constant pressure drop, we note from equation A-3 that  $W/W_o = 1 - t/\delta_o$ . Therefore, for constant pressure drop across a single tube row

$$u_o/u = 1 + (h_o \delta_o/k_p) (t/\delta_o) \quad (A-13)$$

Equations A-12 and A-13 are plotted in Figure 17.

P = 150 PSIA  
Vg = 100 FT/SEC  
D = 1/8 IN.  
Ho = 4320 PPM

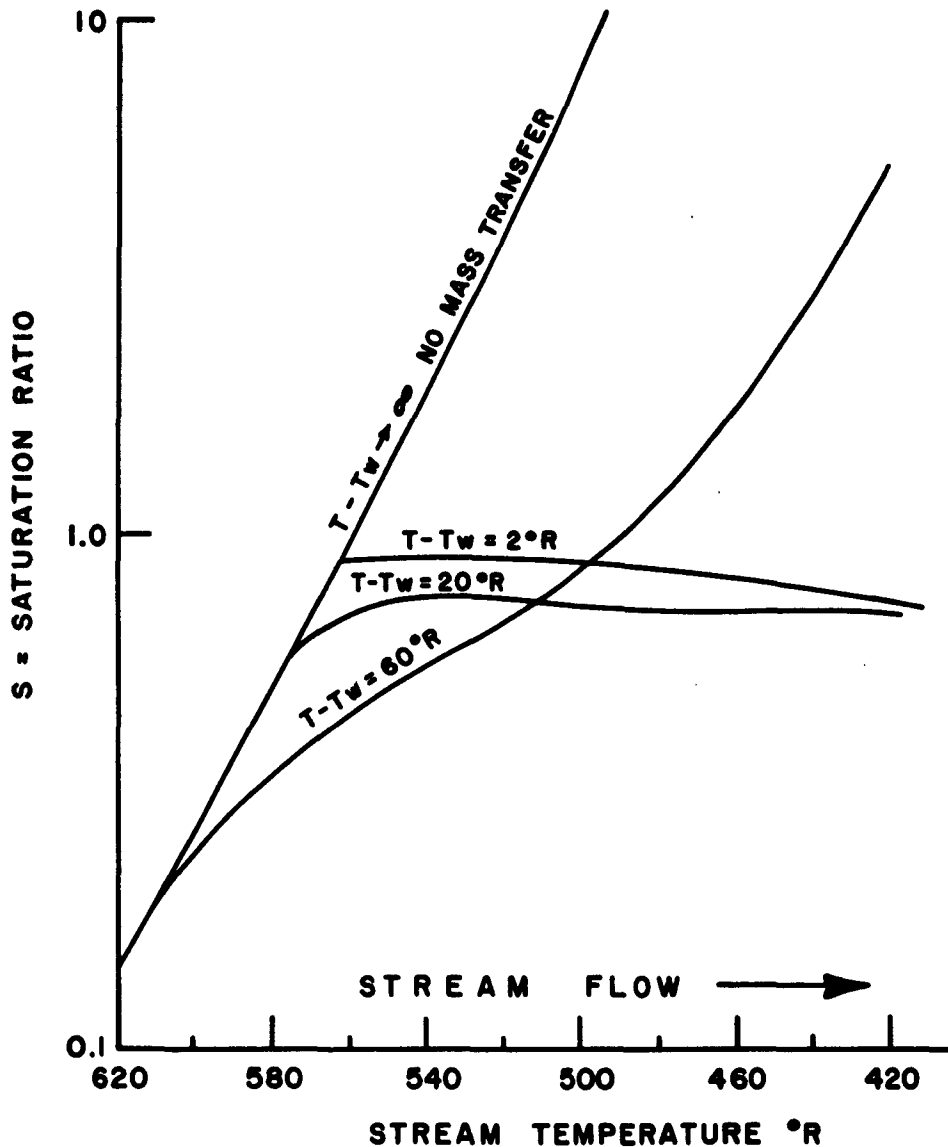


**FIGURE 1**  
**EFFECT OF WATER VAPOR REMOVAL BY MASS TRANSFER**  
**TO TUBE WALLS ON SATURATION RATIO**



FIGURE 2  
TEST- SKID  
VIEWING SIDE

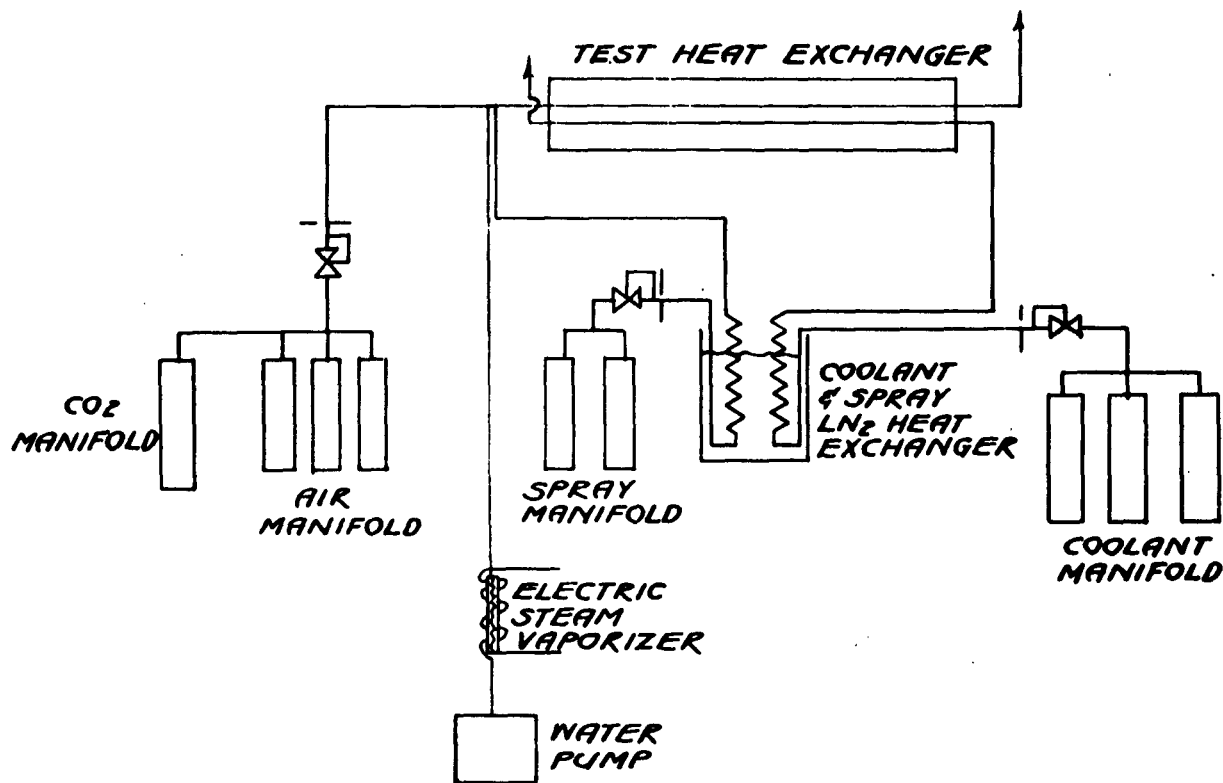


FIGURE 3  
TEST FACILITY SCHEMATIC

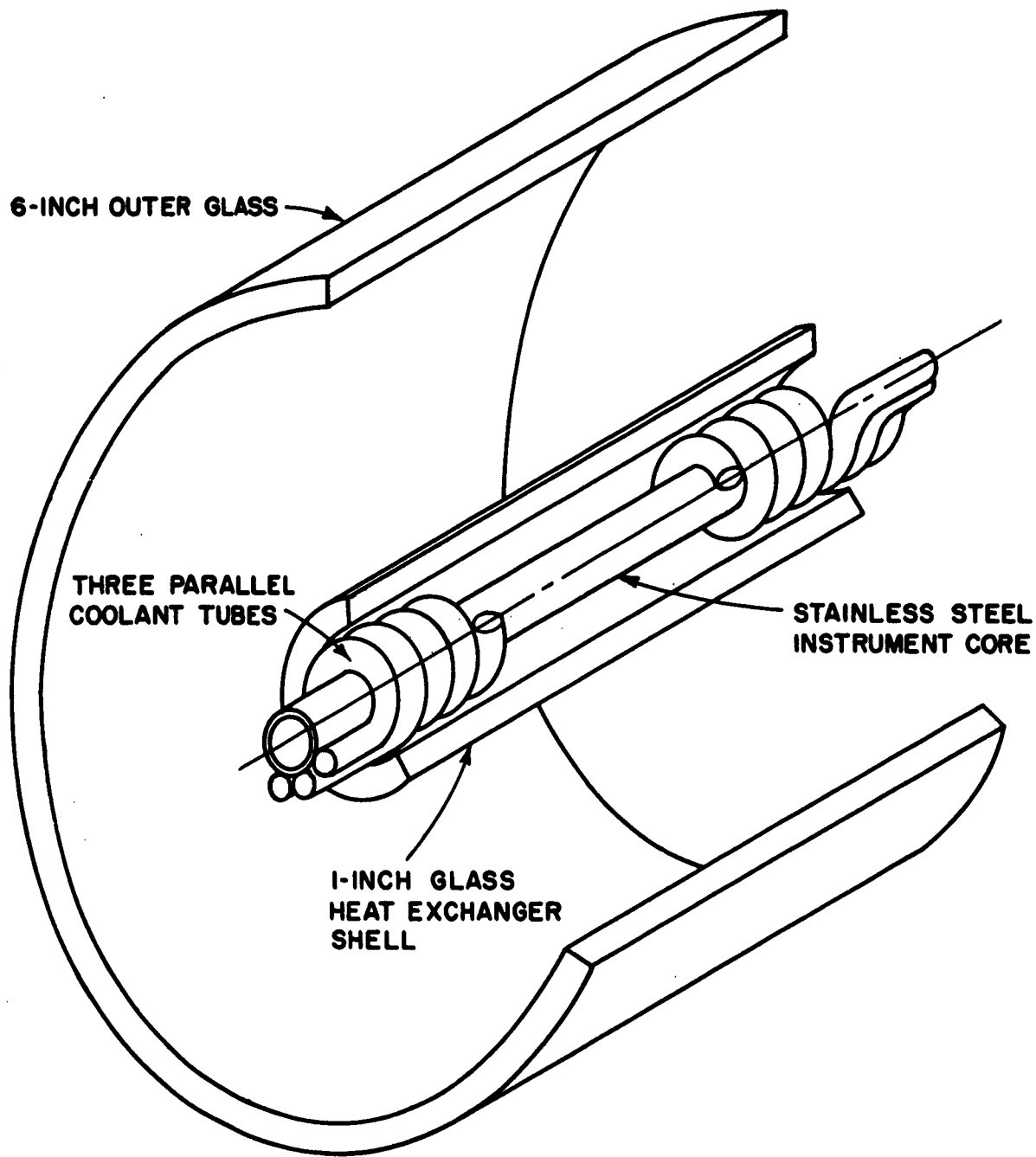


FIGURE 4  
TEST CORE WRAP-UP

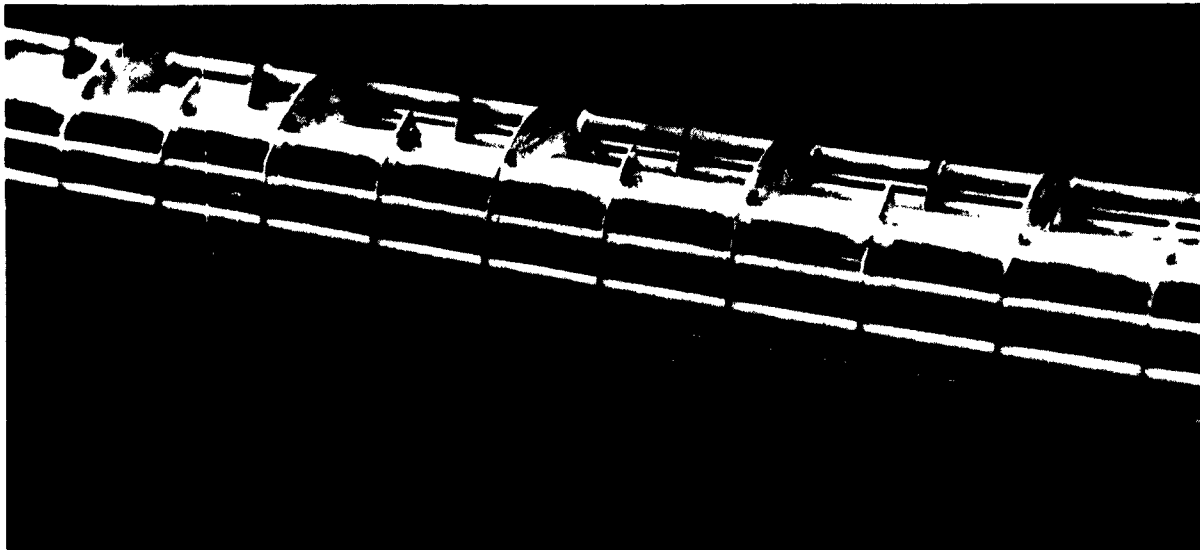


A. OUTER GLASS ON ALIGNMENT CHANNEL WITH FLANGES AND 2-INCH INNER GLASS INSTALLED.

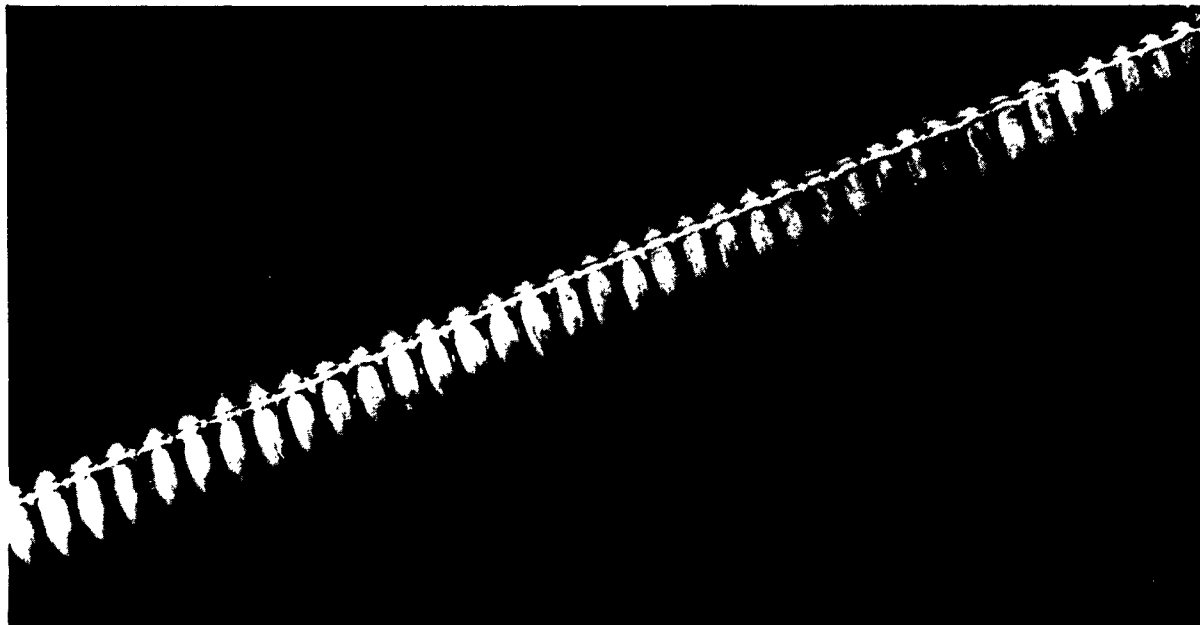


B. TEST CORE FOR 1-INCH SPIRAL HEAT TRANSFER SECTION (1-INCH SPIRAL COOLANT TUBES, WITH INSTRUMENTATION CORE AND TYPICAL 1-INCH INNER GLASS)

FIGURE 5  
TEST HEAT EXCHANGER



**A 2-INCH STAGGERED TUBE BAFFLED HEAT EXCHANGER  
TUBE AND BAFFLE DETAILS**



**B 2-INCH SPIRAL TUBE HEAT EXCHANGER  
TUBE DETAILS**

**FIGURE 6**

**TEST HEAT TRANSFER SECTIONS**

CLOSE - UP AT 21-29 INCHES  
TEST F-17

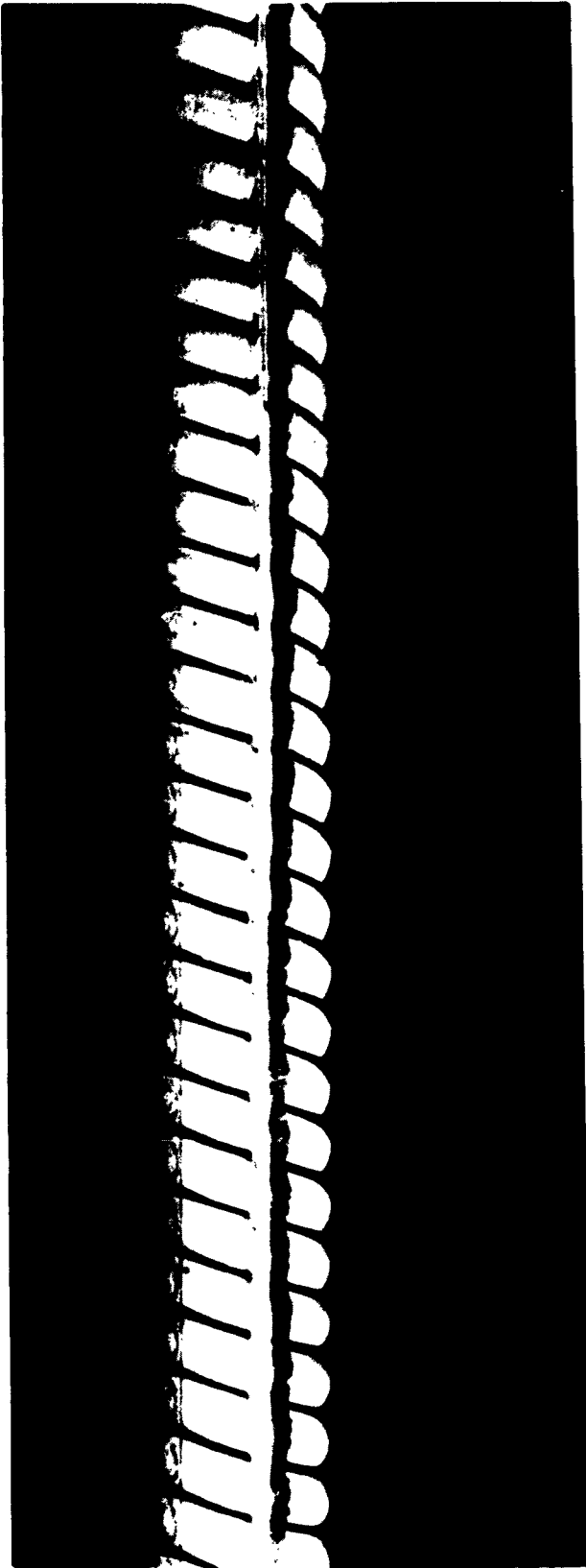
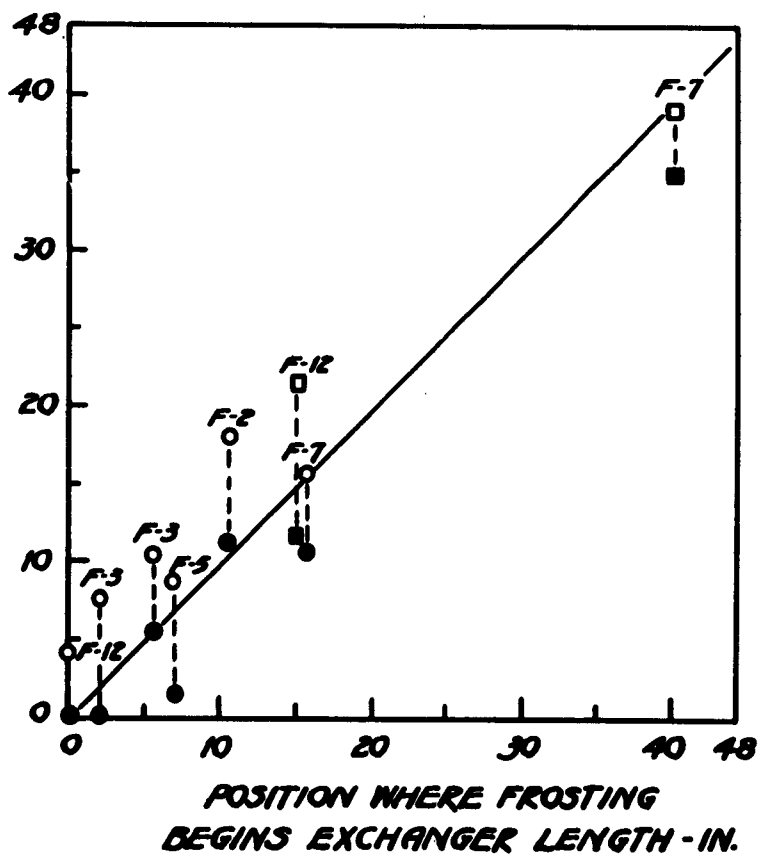


FIGURE 7  
"MASS DIFFUSION" DEPOSIT FORMATION

EXCHANGER LENGTH AT WHICH TEMPERATURE  
(GAS OR WALL) REACHES SATURATION TEMP.

**LEGEND:**

- - H<sub>2</sub>O FROST, AIR TEMP.
- - " " , WALL "
- - CO<sub>2</sub> FROST, AIR TEMP.
- - " " , WALL "



**FIGURE 8**  
**LOCATION OF FREEZE-OUT POINT**

CLOSE-UP AT 2-10 INCHES  
TEST F-13

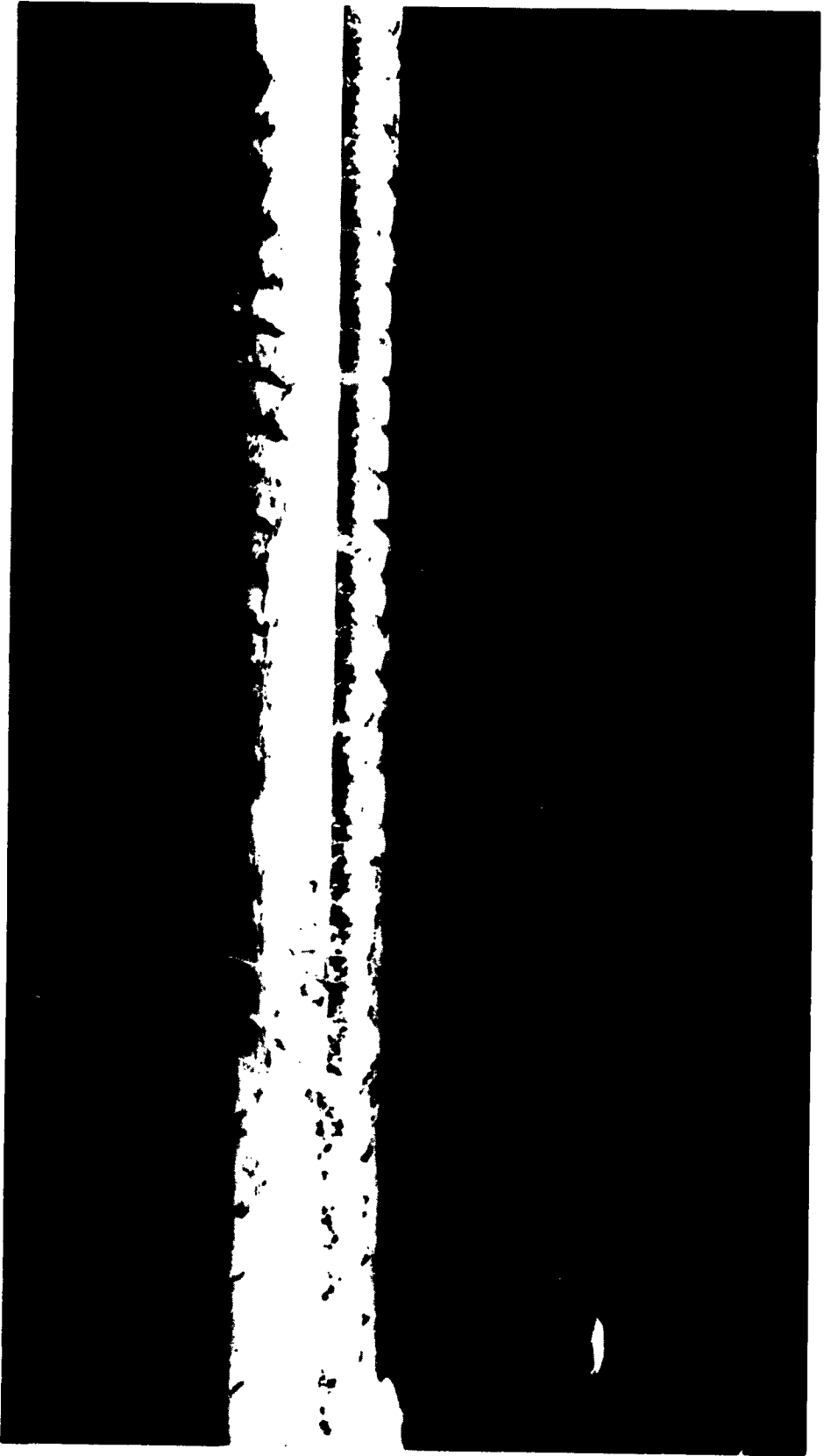


FIGURE 9  
"LN<sub>2</sub> SPRAY" DEPOSIT FORMATION

CLOSE - UP AT 0-8 INCHES  
TEST F-12

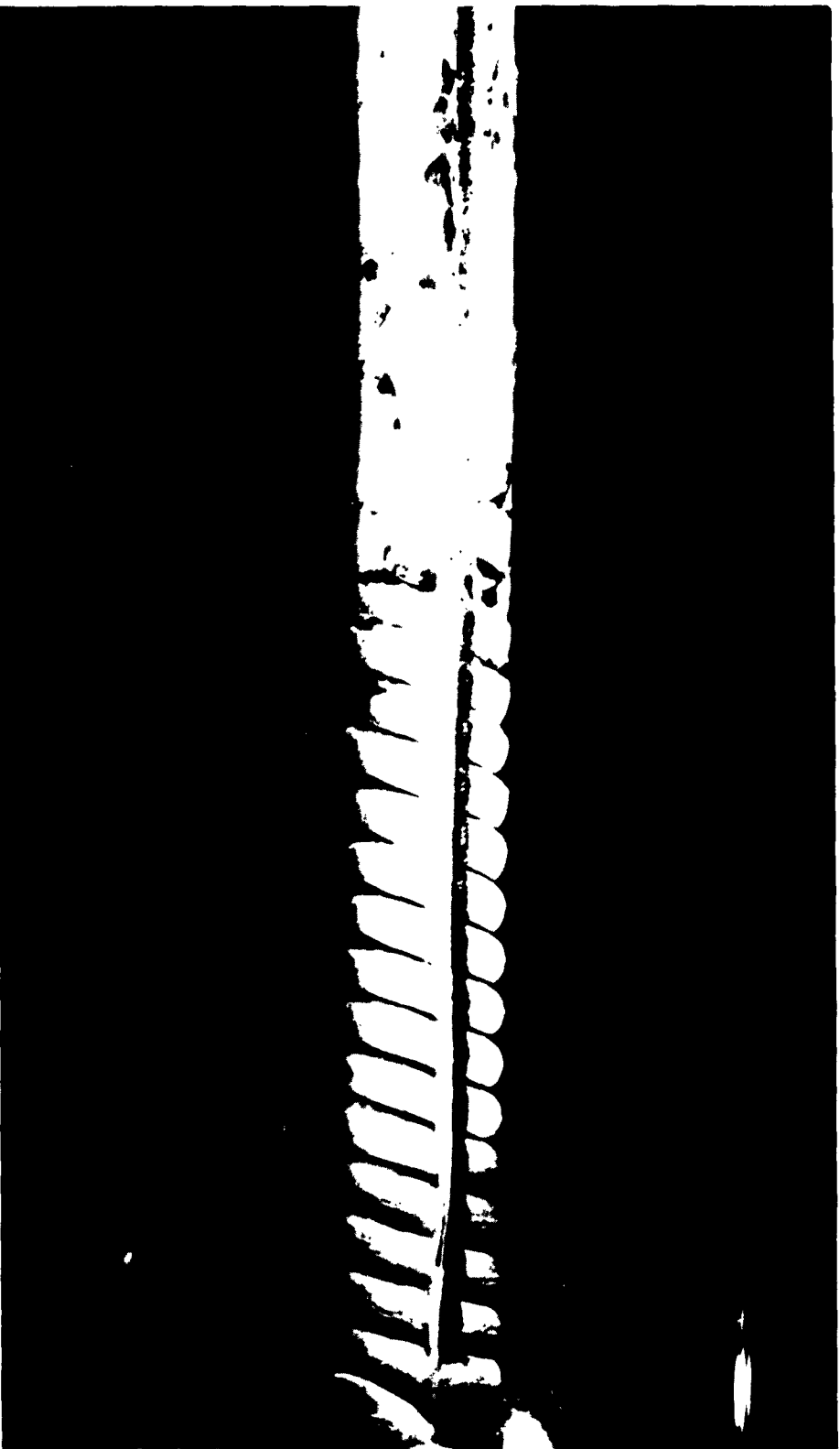
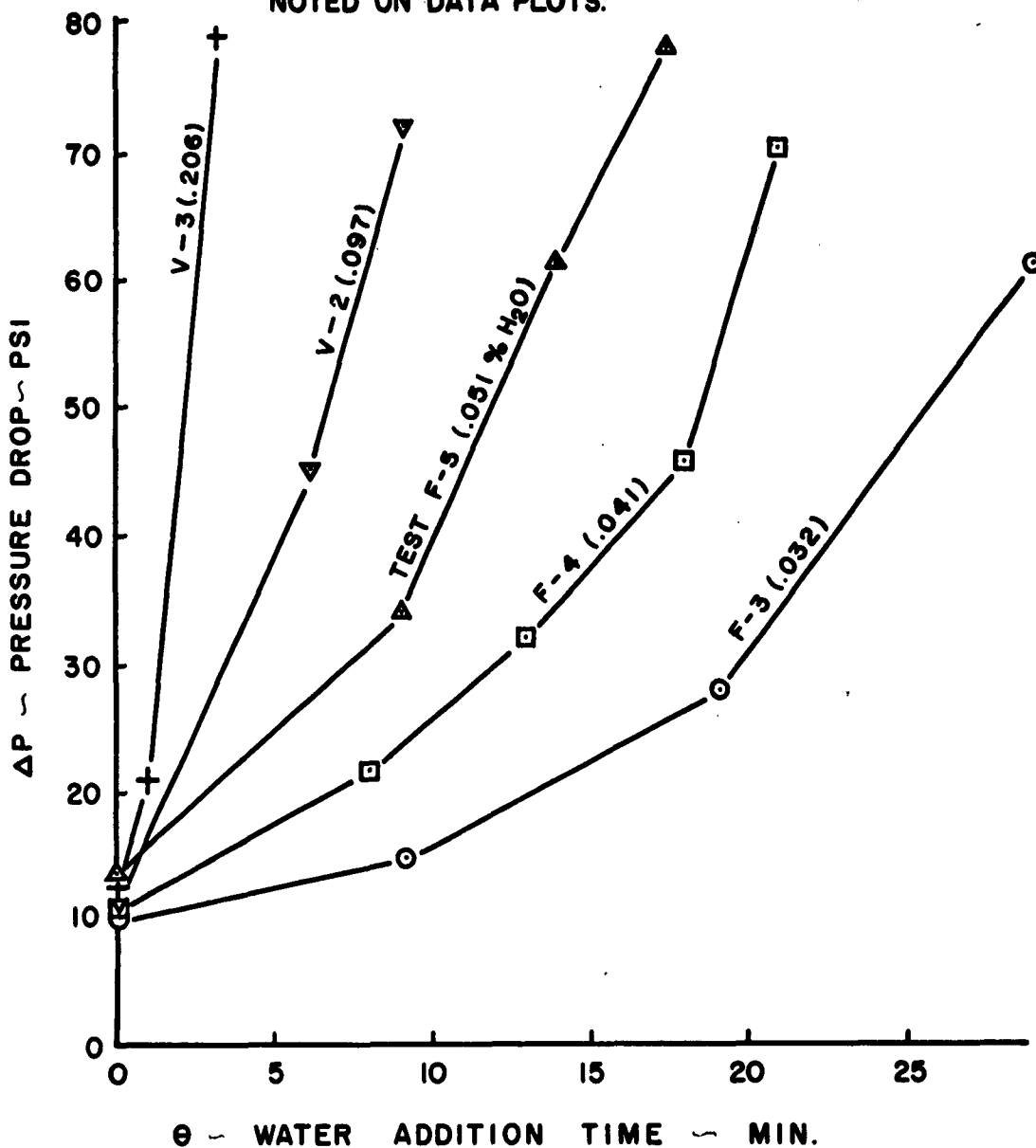


FIGURE 10  
"HIGH  $\Delta T$ " DEPOSIT FORMATION

**NOTES:**

1. ALL TESTS SIMILAR EXCEPT FOR WATER CONTENT  
 $G=30 \text{ LB/SECFT}^2$ ,  $P=90 \text{ PSIA}$ ,  $\% \text{CO}_2\text{H}_2\text{O}$
2. TEST NUMBER AND WATER CONTENT (% BY WEIGHT)  
NOTED ON DATA PLOTS.



**FIGURE II**  
**TYPICAL PRESSURE DROP DATA**

SYMBOL	TEST	%H <sub>2</sub> O	G LB/SECFT <sup>2</sup>	P PSIA	COOLANT INLET TEMP-°R	x/L
●	DATA of FIG. 11		30	90	300	.32-.37
▲	F-17	.017	100	300	150	.30
⊙	F-8	.016	30	90	170	.23
□	V-8	.025	15	90	170	.18
△	F-10	.018	50	90	170	.18
+	V-1	.025	10	30	190	.17
▽	V-5	.027	30	90	410	.44

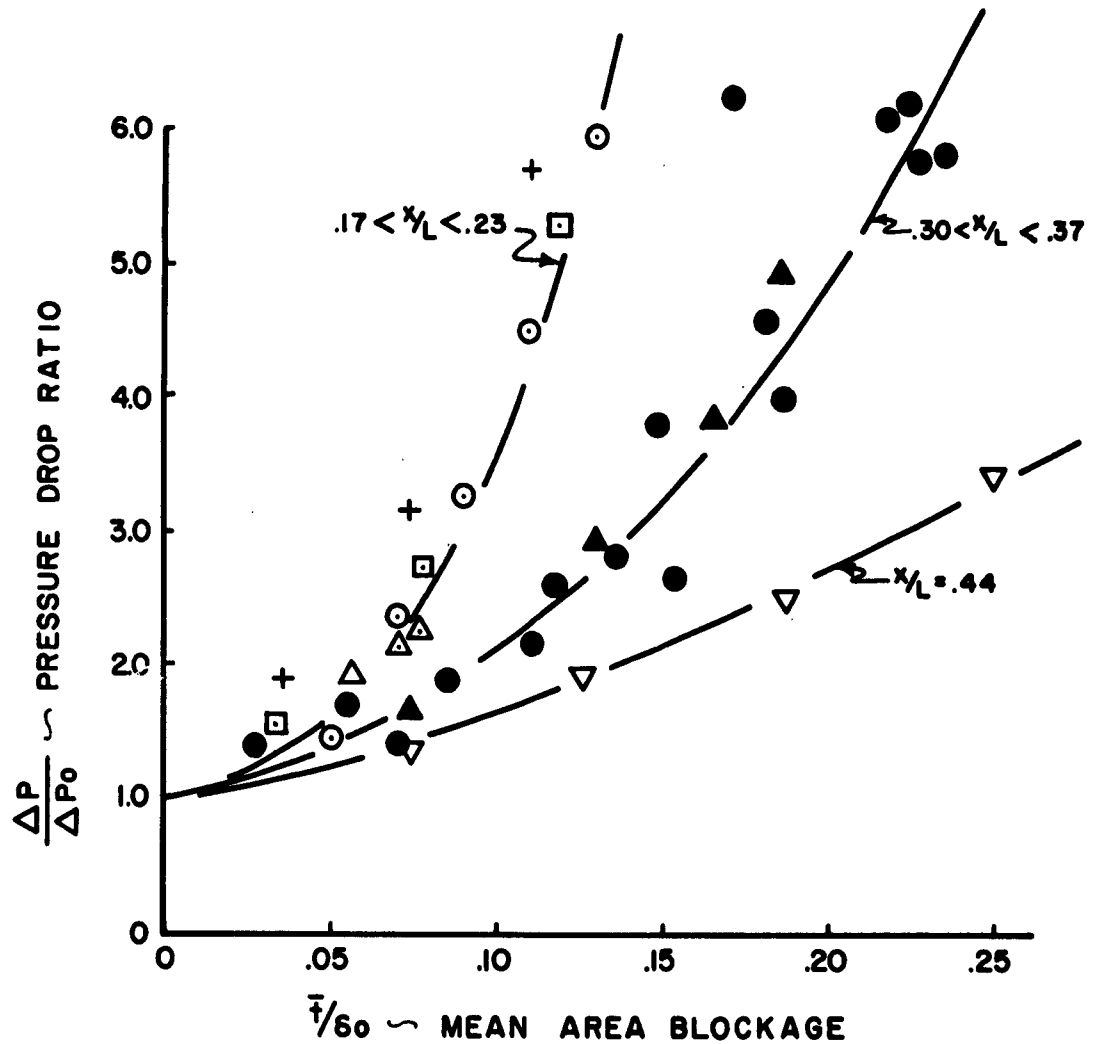


FIGURE 12  
PRESSURE DROP CORRELATION

<u>SYMBOL</u>	<u>TEST</u>	<u>W<sub>SPRAY</sub></u> <u>W<sub>CARRIER</sub></u>
■	F-14	.25
●	F-13	.33
▼	V-9	.46

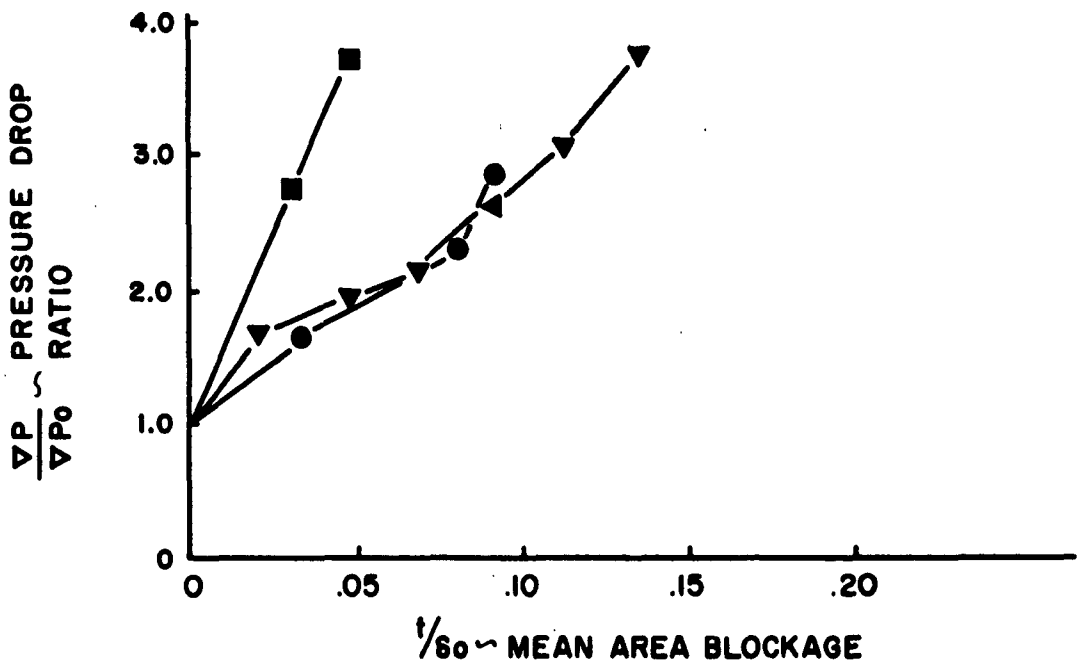


FIGURE 13

PRESSURE DROP CORRELATION  
LN<sub>2</sub> SPRAY TESTS

<u>SYMBOL</u>	<u>TEST</u>	<u>% H<sub>2</sub>O</u>
+	F-2	.006
○	F-3	.032
□	F-4	.041
▲	F-5	.051

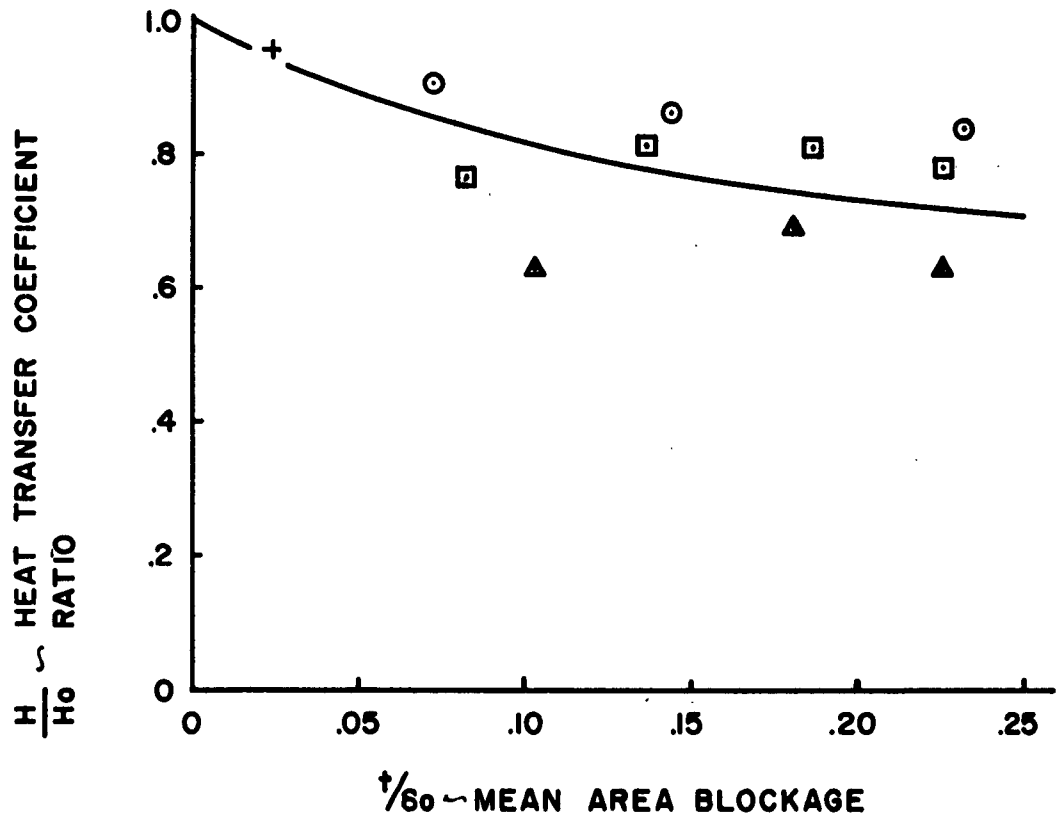
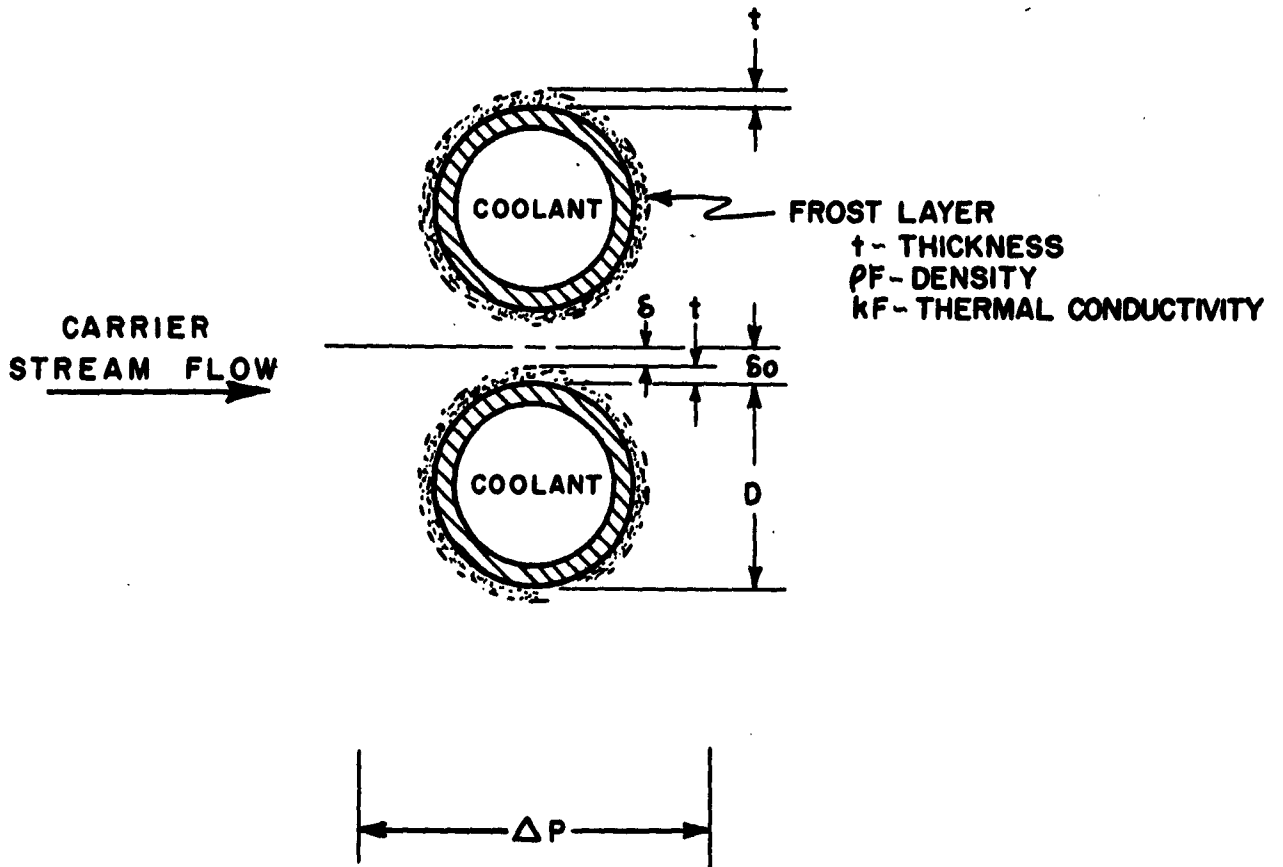


FIGURE 14  
HEAT TRANSFER CORRELATION



**FIGURE 15**  
**GEOMETRIC MODEL FOR SINGLE TUBE**  
**FLOW AND HEAT TRANSFER ANALYSIS**

**NOTES:**

1. CONSTANT FLOW DENSITY

2. 
$$\frac{\Delta P/\Delta P_0}{(w/w_0)^2} = \left[ \frac{1}{1-t/s_0} \right]^2$$

3. RESULTS APPLICABLE TO ANY SYSTEM OPERATING LINE (I.E. CONST.  $w$  or CONST.  $\Delta P$ )

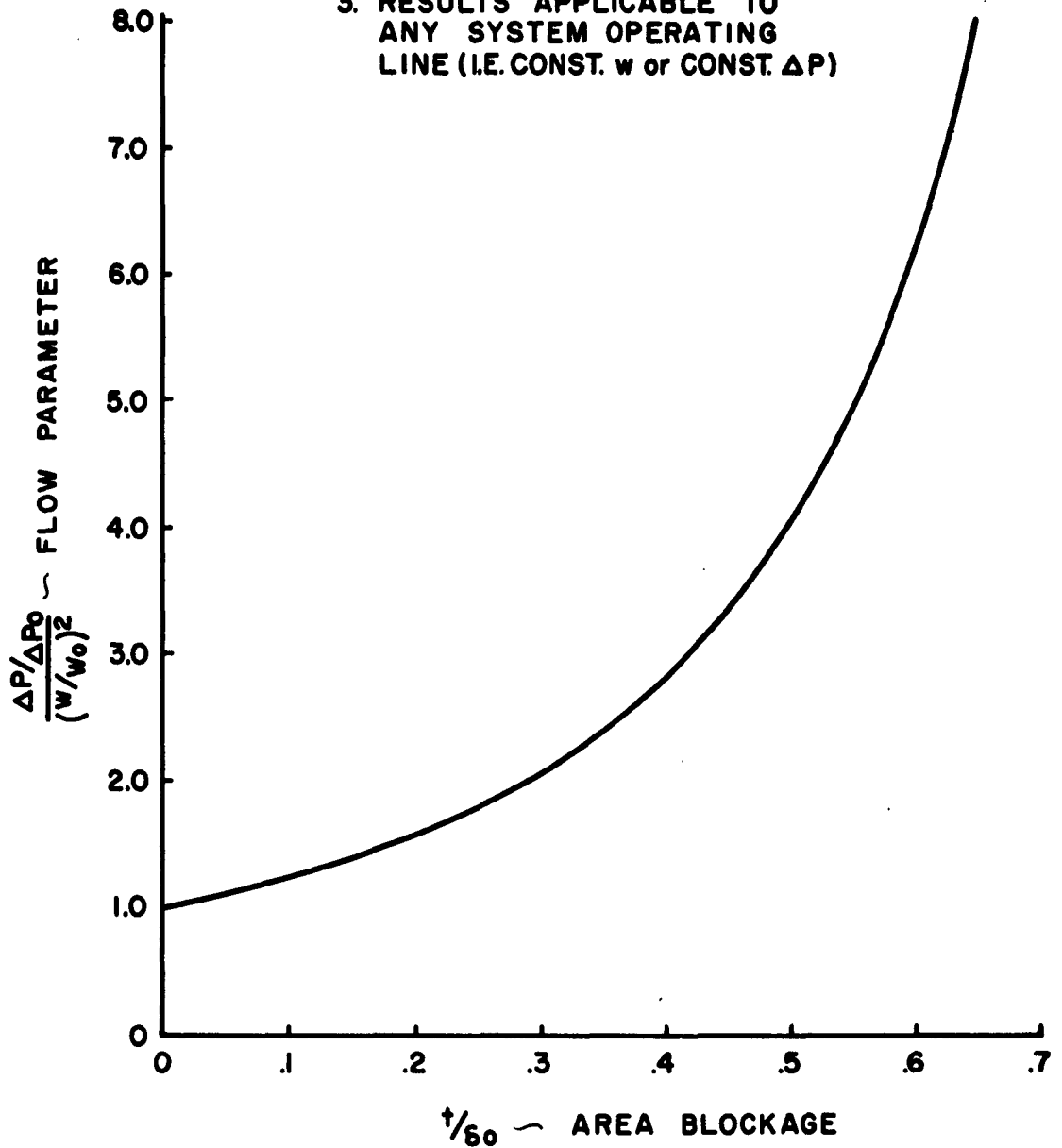


**FIGURE 16**  
**EFFECT OF AREA BLOCKAGE ON FLOW CAPACITY**  
**SINGLE TUBE ROW ANALYSIS**

**NOTES:**

1. CLOSE PACKED TUBES ( $\delta_0/\delta_0 \ll 1$ )

2. FOR CONST  $\Delta P$

$$u_0/u = 1 + \frac{(ho\delta_0)}{RF} (t/\delta_0)$$

3. FOR CONST  $w$

$$u_0/u = (1 - t/\delta_0)^{.6} + \frac{(ho\delta_0)}{RF} (t/\delta_0)$$

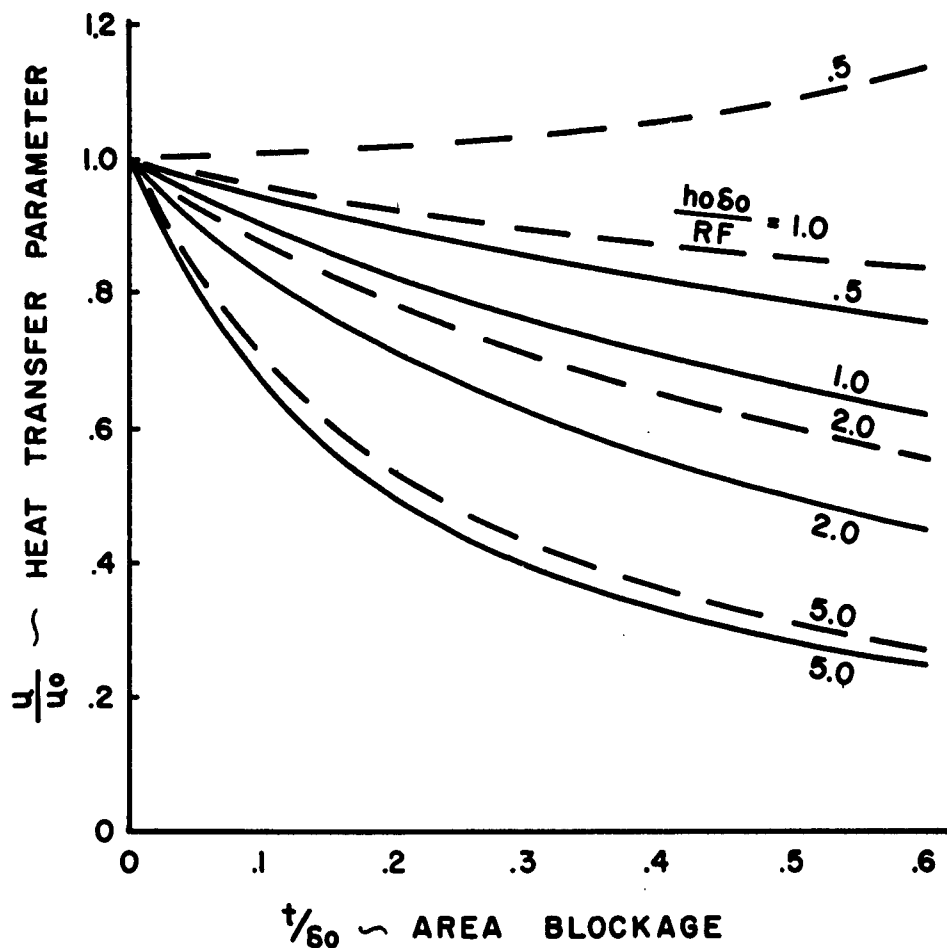


FIGURE 17

**EFFECT OF FROST LAYER ON HEAT TRANSFER  
SINGLE TUBE ROW ANALYSIS**

- MIT DATA (PLATE ~140°R)
- NACA TN 3143 (PLATE ~460°R)
- x ADL DATA (FROM TESTS F-17 & V-2)

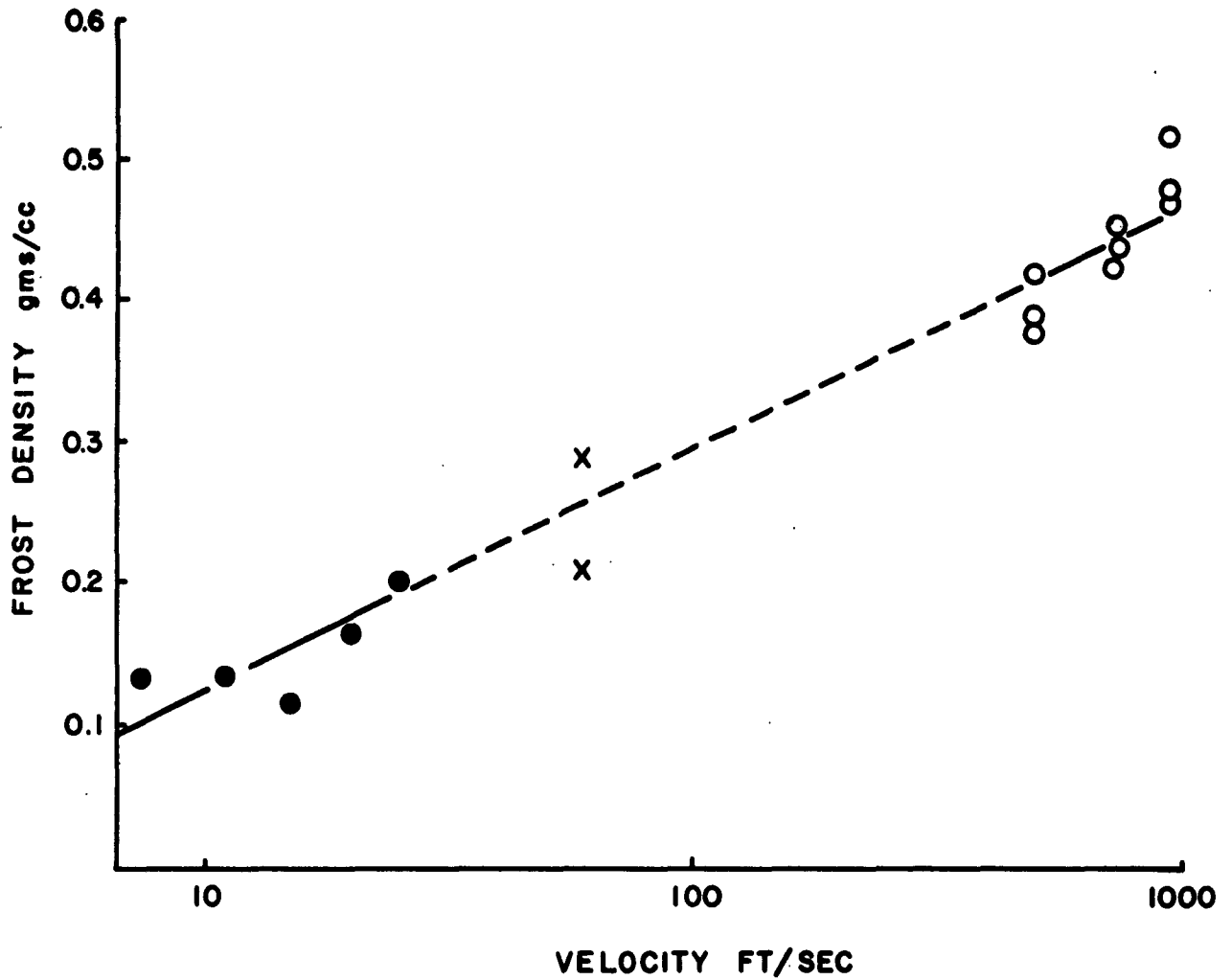
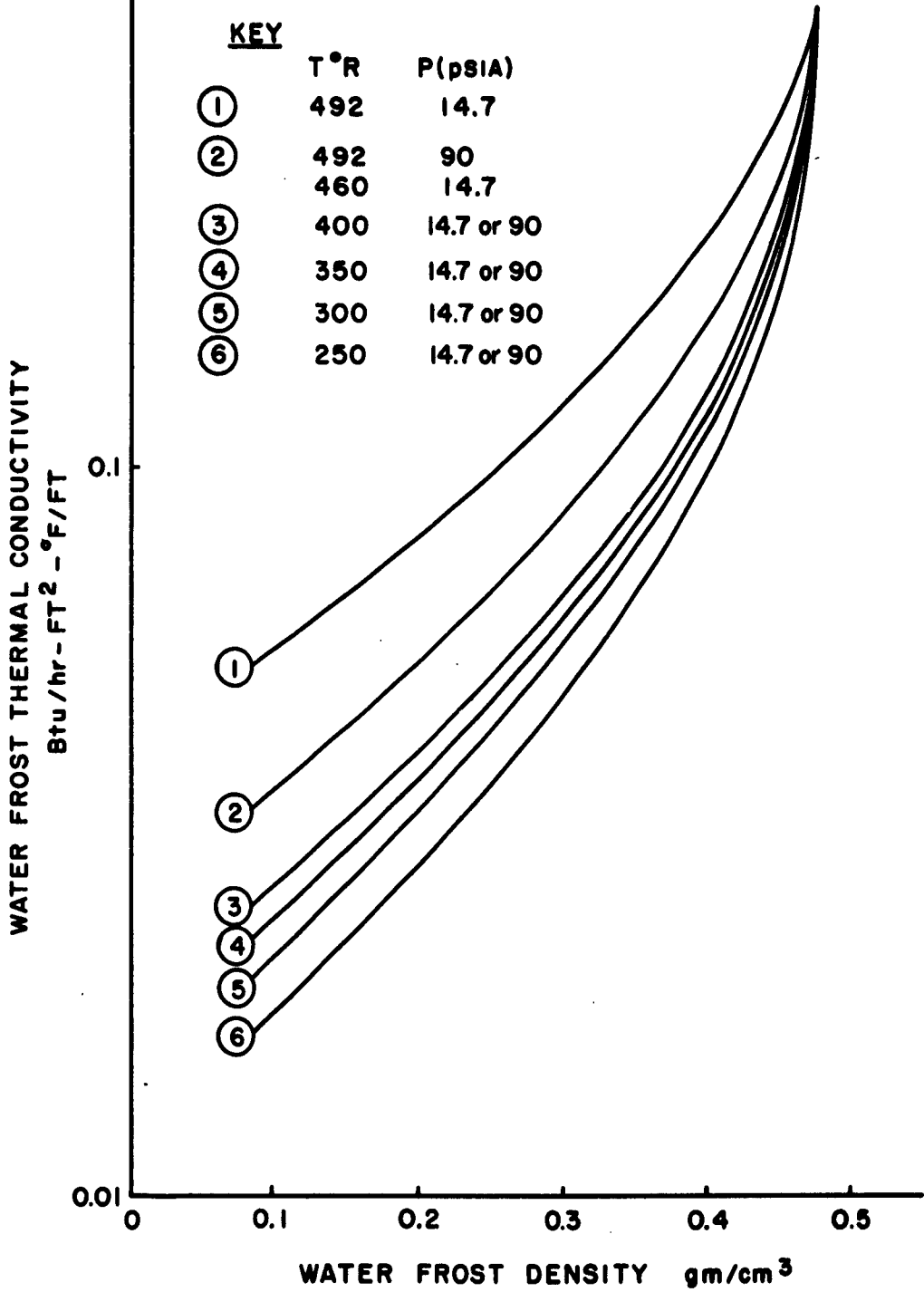


FIGURE 18  
WATER FROST DENSITY

**NOTE:**

**CALCULATED BY WOODSIDE MODEL**



**FIGURE 19**  
**LOW-DENSITY WATER FROST THERMAL CONDUCTIVITY**

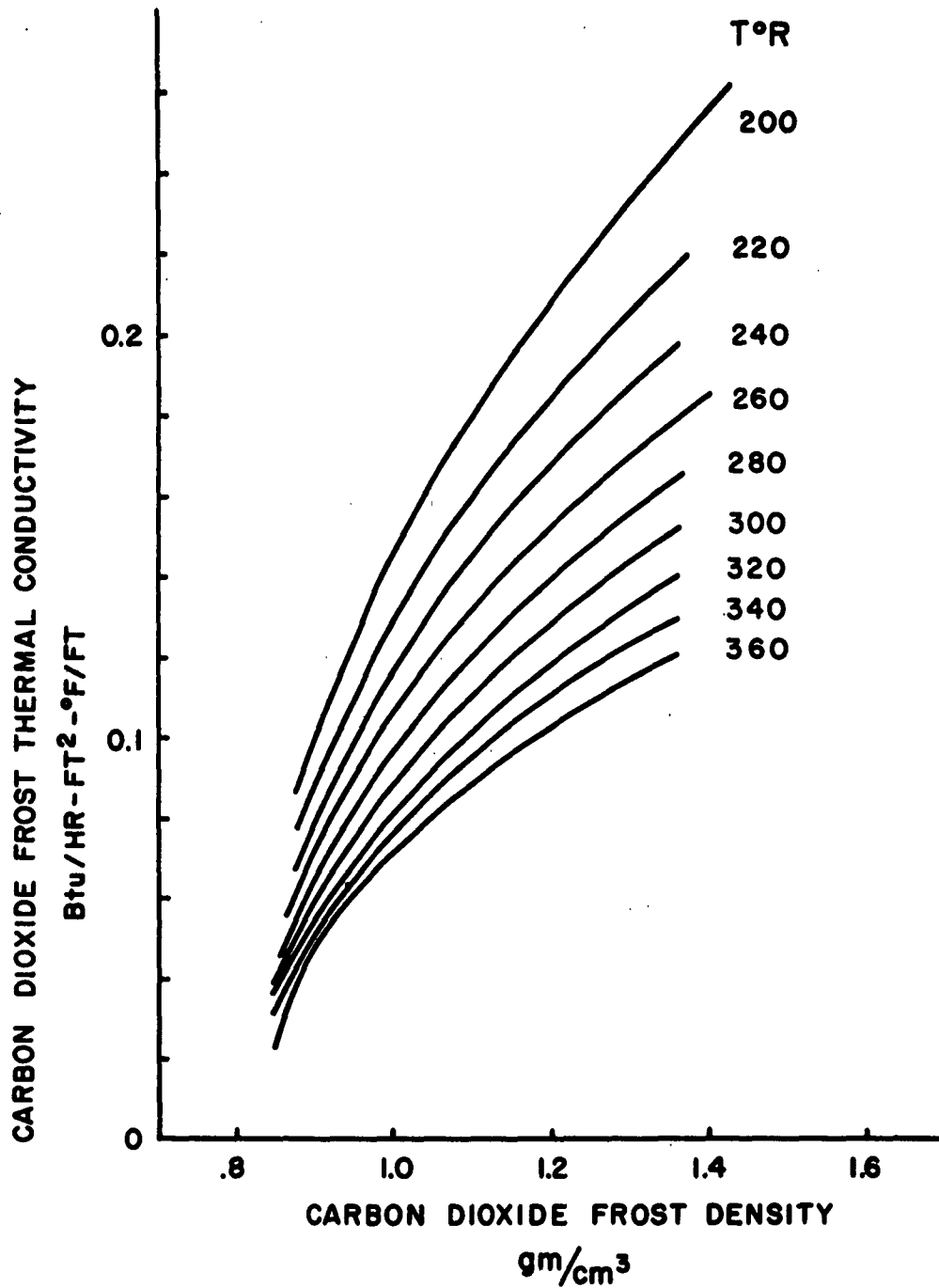


**FIGURE 20**  
**THERMAL CONDUCTIVITY OF CARBON DIOXIDE FROST**

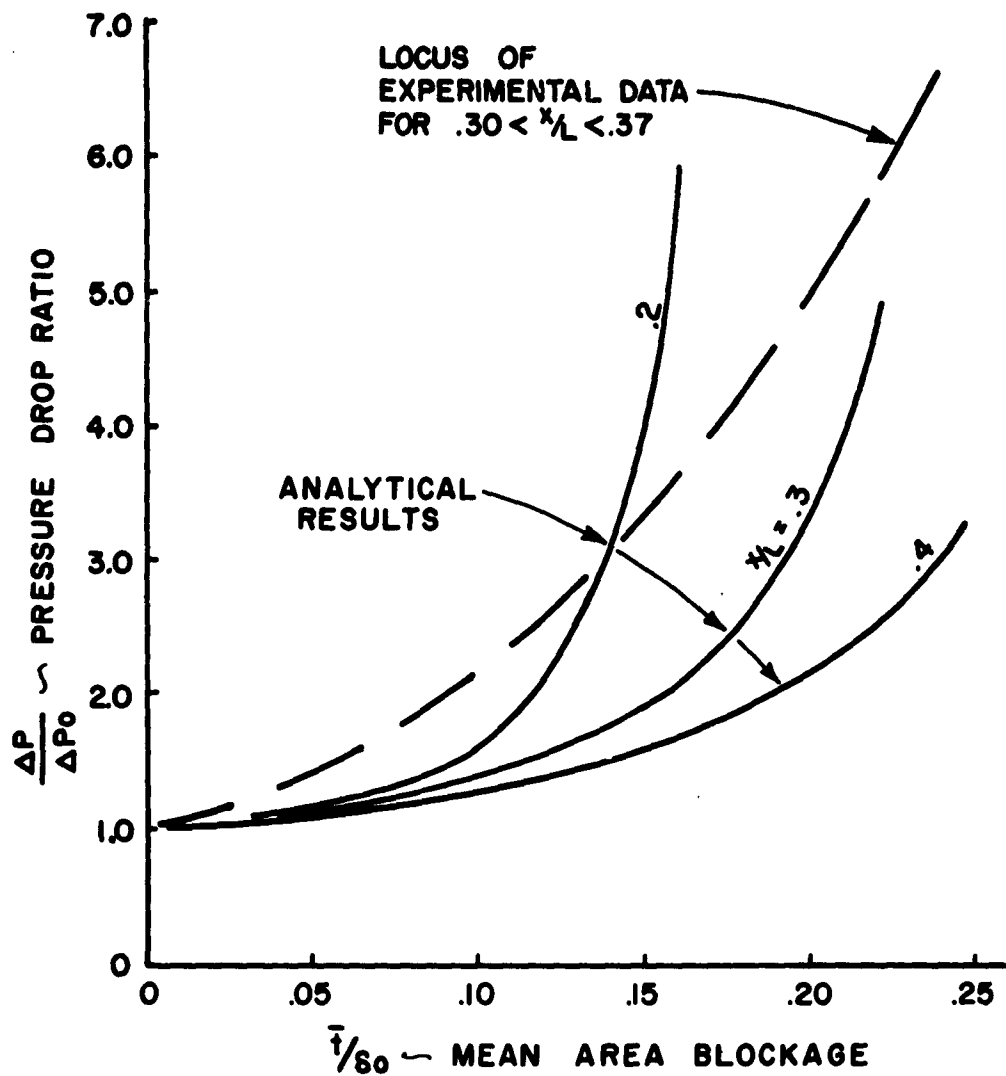


FIGURE 21

OVERALL PRESSURE DROP VS MEAN AREA BLOCKAGE  
COMPARISON OF SIMPLIFIED HAND CALCULATION  
SOLUTION WITH EXPERIMENTAL DATA

● TEST DATA OF FIGURE 14

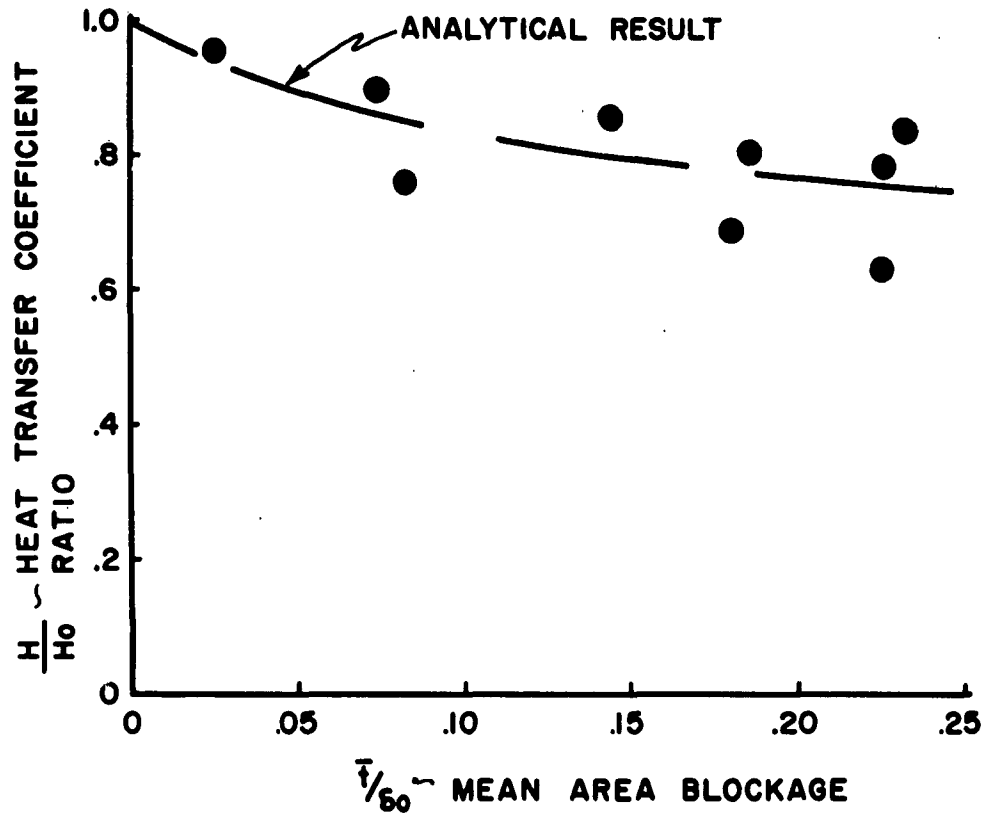
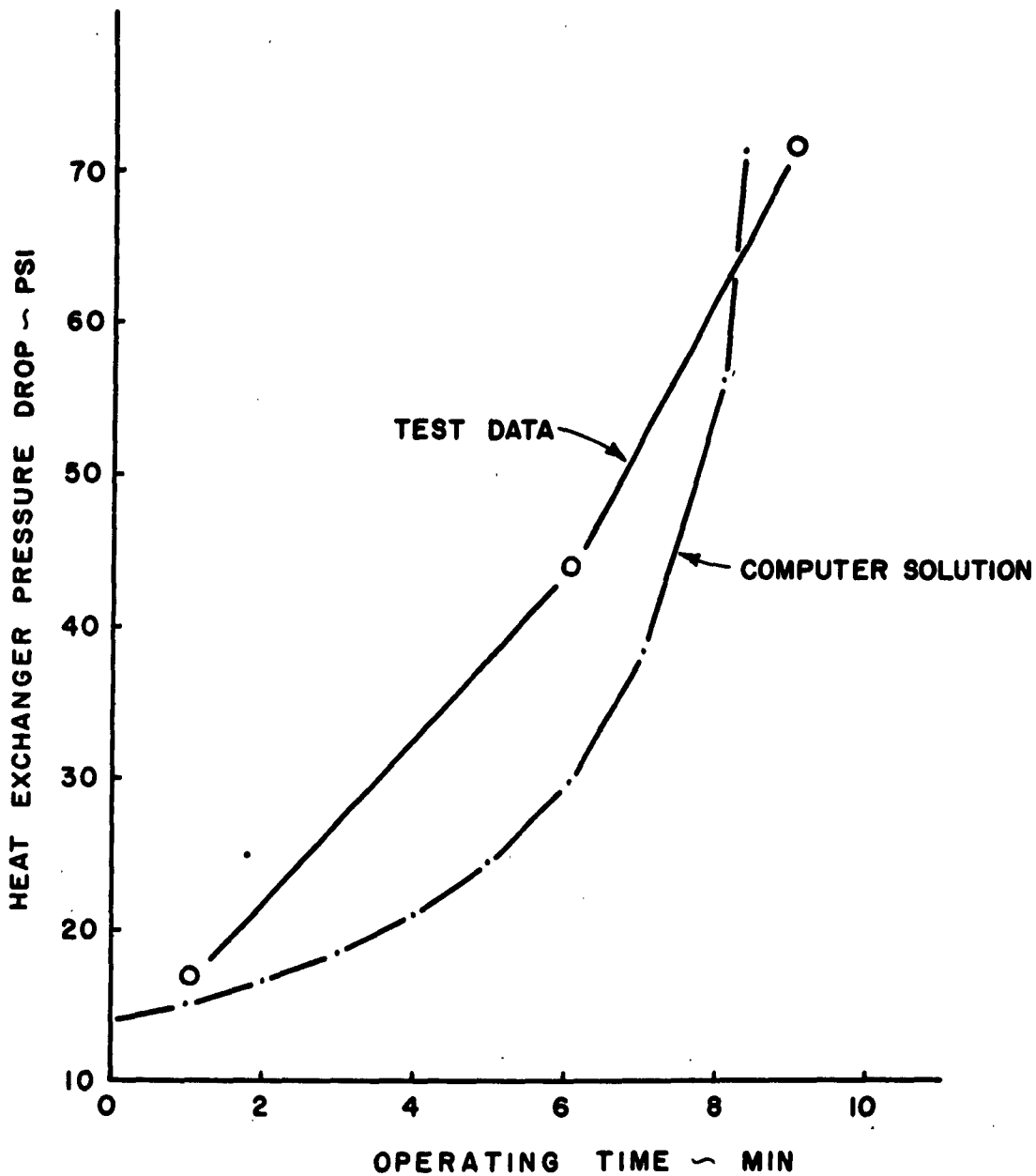
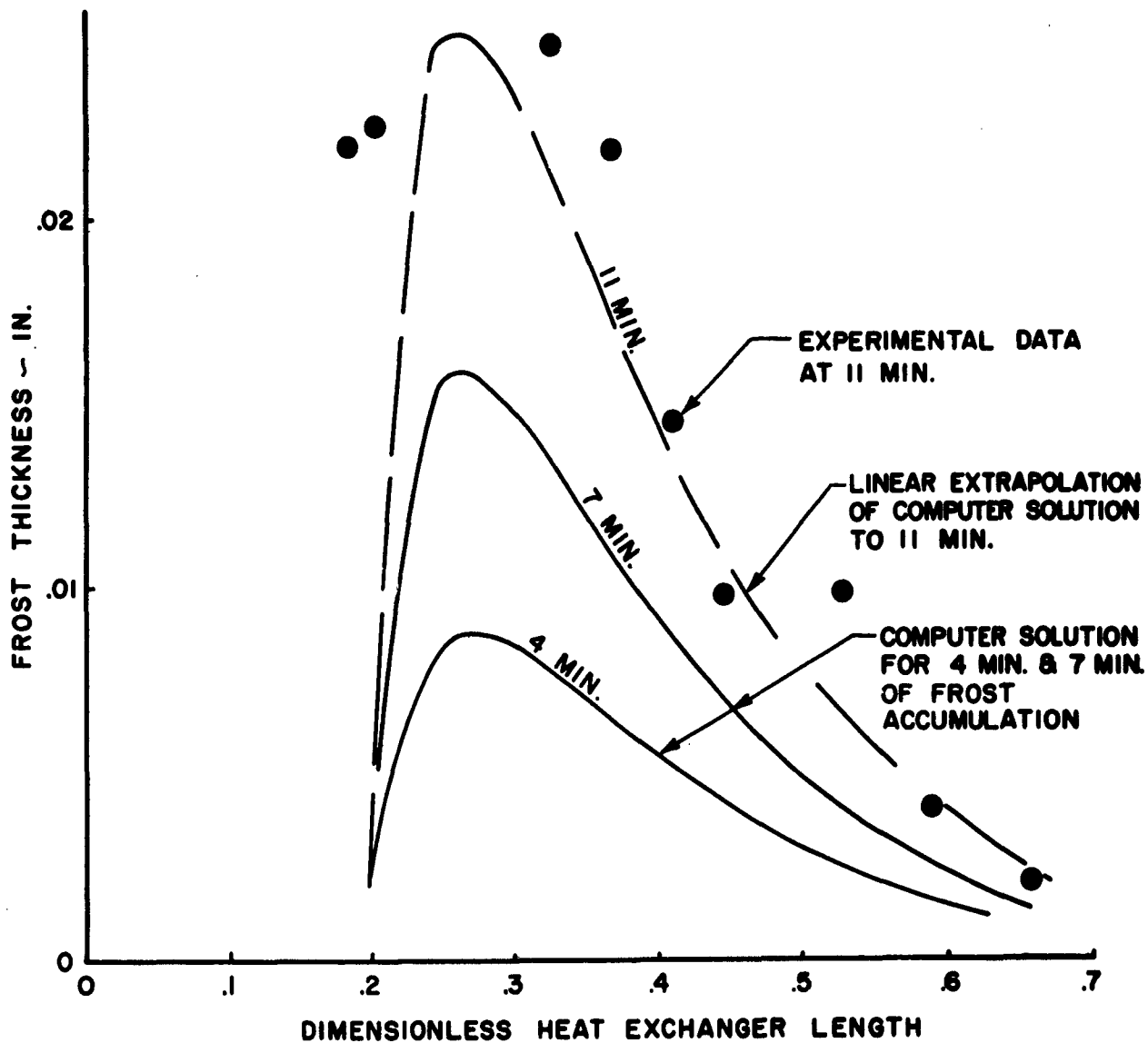


FIGURE 22

OVERALL HEAT EXCHANGER HEAT TRANSFER  
COEFFICIENT - COMPARISON OF SIMPLIFIED  
ANALYTICAL SOLUTION AND EXPERIMENTAL DATA



**FIGURE 23**  
COMPARISON OF PRESSURE DROP TEST DATA WITH  
MASS DIFFUSION COMPUTER PROGRAM



**FIGURE 24**  
COMPARISON OF FROST THICKNESS PROFILE TEST DATA WITH  
MASS DIFFUSION COMPUTER PROGRAM